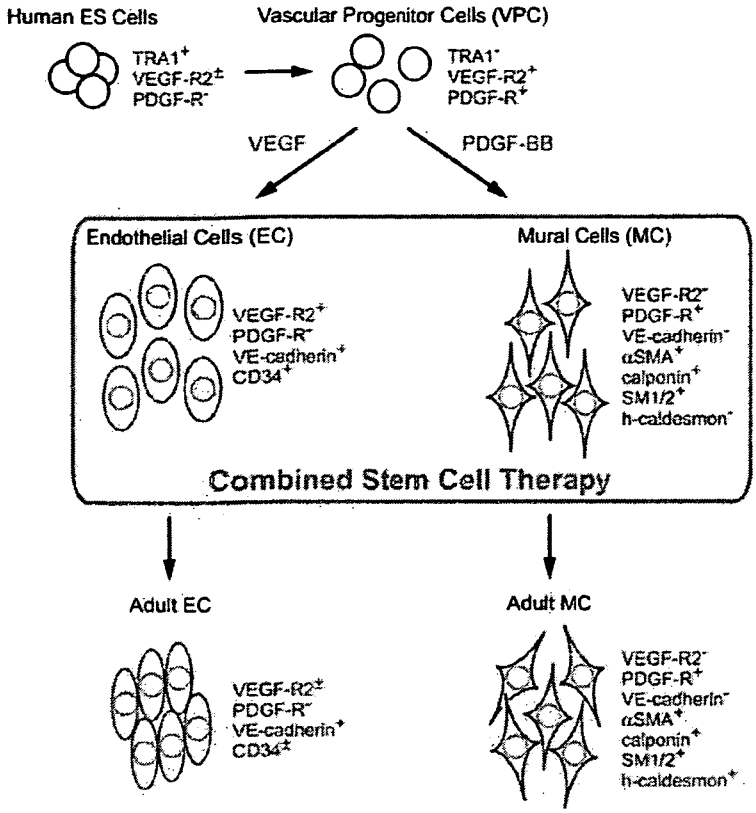

Figure 3. Possible differentiation pathway of vascular cells from human ES cells via VPC.
doi:10.1371/journal.pone.0001666.g003

We further investigated the contribution of transplanted VPC-derived MC to the recruitment of mural cells. We stained the sections of ischemic hindlimbs at day 14 with anti-human SM1 and αSMA antibodies. In EC+MC-transplanted mice, we found some human SM1 and αSMA double positive cells, which were localized within the αSMA positive host vessel wall (Figure 5d: arrow).

Quantification of Transplanted VPC-derived Vascular Cell-induced Vascular Regeneration in Ischemic Hindlimb

The sections of ischemic hindlimbs of the EC+MC group at day 42 were stained with anti-human and mouse CD31 antibodies. Mouse CD31 positive capillary density was significantly high in the EC+MC group ($1775.3\pm54.2/mm^2$), compared to other groups ($P<0.0001$ vs. control group: $1318.6\pm73.0/mm^2$) (Figure 6b). Human CD31 positive capillary density in mice transplanted with human VPC-derived EC (EC ($149.9\pm12.3/mm^2$) and EC+MC ($135.7\pm13.7/mm^2$) was significantly higher than that in mice transplanted with EPC ($95.7\pm8.5/mm^2$ in the pEPC and $115.2\pm12.0/mm^2$ in the uEPC group) ($P<0.05$). Compatible with the result of blood flow measurement, mouse and/or human CD31 positive capillary density markedly increased in mice that received human VPC-derived EC+MC ($1856.8\pm57.0/mm^2$) ($P<0.0001$, compared to the control group ($1318.6\pm73.0//mm^2$)), and also to other groups. Among the single cell transplantation groups, mouse and/or human CD31 positive capillary density increased in the EC group ($1601.4\pm51.4/mm^2$) ($P=0.0016$) compared to the control group, but did not increase in the MC ($1471.8\pm42.4/mm^2$) or EPC groups ($1403.5\pm84.4/mm^2$ in the pEPC and $1524.8\pm108.2/mm^2$ in the uEPC group).

To confirm the maturity of newly formed vessels, we performed the immunostaining of the ischemic tissues with anti-αSMA antibody, which could stain both human and mouse MC (Figure 6c). We confirmed that αSMA positive capillary density was significantly increased in the human VPC-derived vascular cells-transplanted groups (MC ($1317.6\pm45.4/mm^2$), EC ($1357.7\pm27.3/mm^2$) and EC+MC ($1554.9\pm48.8/mm^2$)) ($P<0.0001$), compared to the control group ($1021.3\pm46.3/mm^2$) (Figure 6d). Among the EPC groups, αSMA positive capillary density was significantly increased in the uEPC group ($1185.7\pm42.2/mm^2$) ($P<0.0076$) compared to the pEPC ($1118.9\pm36.8/mm^2$) and control group. We further investigated the extent of arteriogenesis in these groups using αSMA immunostaining sections. Many αSMA positive arterioles with more than 20 μm in diameter were detected in the EC+MC group, but not in the control group (Figure 6c: arrowhead). The number of αSMA positive arterioles significantly increased in the human VPC-derived vascular cells-transplanted groups, especially in the EC+MC group (the MC group:$4.0\pm0.3/mm^2$ and the EC group:$3.7\pm0.2/mm^2$; $P<0.001$, compared to the control group: $2.0\pm0.2/mm^2$, the EC+MC group: $5.5\pm0.7/mm^2$; $P<0.0001$, compared to all other groups) (Figure 6e). However, no significant difference in the number of αSMA positive arterioles was seen between the EPC (the pEPC group:$1.9\pm0.2/mm^2$ and the uEPC group:$2.0\pm0.2/mm^2$) and control groups.

Discussion

The present study demonstrated that the transplantation of human VPC-derived vascular cells at the proper differentiation

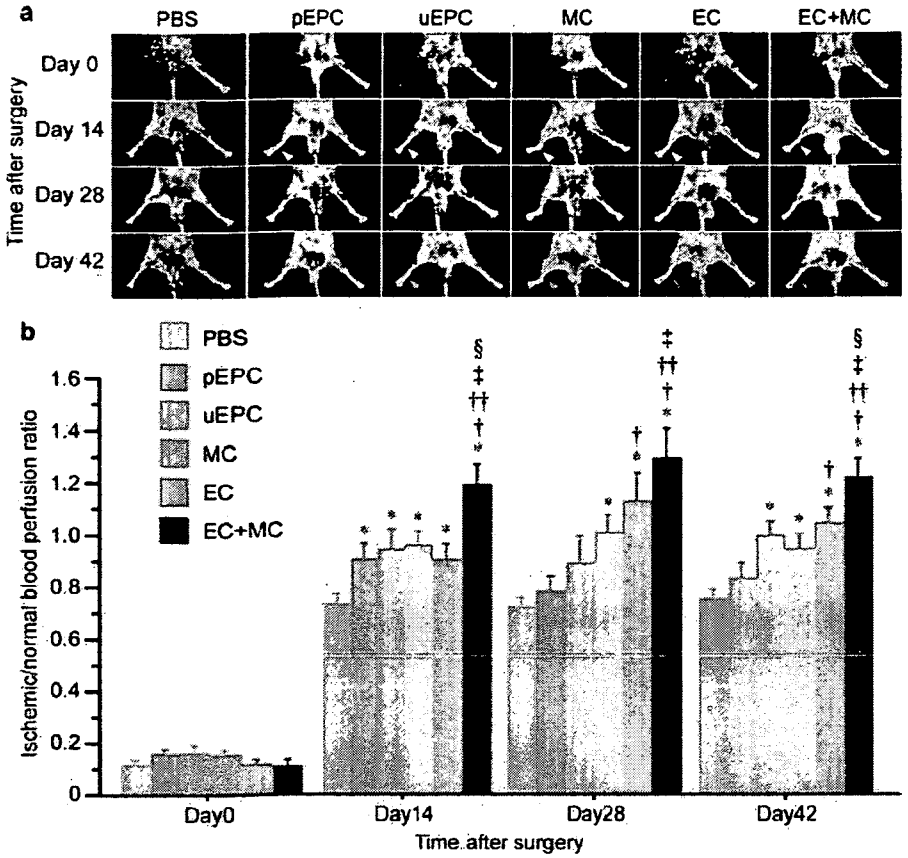

Figure 4. Augmented vascular regeneration by intra-arterial transplantation of human VPC-derived vascular cells in a murine hindlimb ischemia model. a) Serial LDPI analysis in hindlimb ischemia mice. At day 14, the blood flow of ischemic limbs in all cell transplanted groups increased significantly compared to the control group (white arrowhead). After 42 days, significant blood flow recovery was observed in the uEPC and human VPC-derived EC and/or MC-transplanted groups (red arrowhead), but not in pEPC. b) Quantitative analysis of hindlimb blood flow by calculating the ischemic/normal limb perfusion ratios after the induction of hindlimb ischemia. *$P<0.05$ vs. control, †$P<0.05$ vs. pEPC, ††$P<0.05$ vs. uEPC, ‡$P<0.05$ vs. MC, §$P<0.05$ vs. EC.
doi:10.1371/journal.pone.0001666.g004

stage successfully promoted vascular regeneration in the setting of tissue ischemia. After the expansion of human VPC-derived EC and MC, when intra-arterially administered, these cells significantly augmented neovascularization in an animal model of experimentally-induced hindlimb ischemia, compared to human peripheral blood and umbilical cord-derived EPC (pEPC and uEPC). Furthermore, the combined transplantation of human VPC-derived EC and MC could markedly induce vascular regeneration, compared to the single fraction transplantation of VPC-derived vascular cells (EC or MC). We also succeeded in demonstrating that transplanted human VPC-derived vascular cells were incorporated into the host circulation as both EC and MC. These results indicate that the combined transplantation of human VPC-derived EC and MC may have utility as a novel strategy for vascular regenerative medicine.

In the present study we used human VPC-derived VEGFR2$^+$ VE-cadherin$^+$ cells for the expansion and transplantation of EC. VEGFR2$^+$VE-cadherin$^+$ cells, obtained at day 10 of differentiation, were also positive for CD34 and therefore considered to be EC at the early differentiation stage (Figure 3) [9]. Even after 6 passages, 20~40% of these cells exhibited the expression of VEGFR2, VE-cadherin, and CD34, which indicated that they still retained the phenotype of EC at the early differentiated stage. Compared to EPC, transplantation of these EC significantly augmented ischemia-induced neovascularization. In contrast, we found that ischemia-induced neovascularization was not improved in mice receiving human aortic endothelial cells [4]. Therefore, human VPC-derived EC at the early differentiation stage might possess vascular regenerative capacity and these EC can be a valuable source for promoting vascular regeneration.

After expansion of human VPC-derived VEGFR2$^+$VE-cadherin$^+$ cells, about 70% of the expanded cells were αSMA positive. However, these cells were negative for the mature mural cell markers, including calponin, SM1, SM2, and h-caldesmon (data not shown). In contrast, expanded VEGFR2$^+$ VE-cadherin$^-$ cells obtained from human VPC under platelet derived growth factor (PDGF)-BB stimulation were positive for αSMA, calponin, SM1, and SM2, but negative for h-caldesmon. HAoSMC was positive for all of the mature MC markers, including h-caldesmon. In another series of our experiments, the mice receiving hAoSMC transplantation exhibited no significant improvement of neovascularization after the induction of ischemic hindlimbs (data not shown). Because h-caldesmon and calponin were reported to be expressed relatively late in SMC differentiation [10], human VPC-derived MC might be at a rather early "immature" differentiation

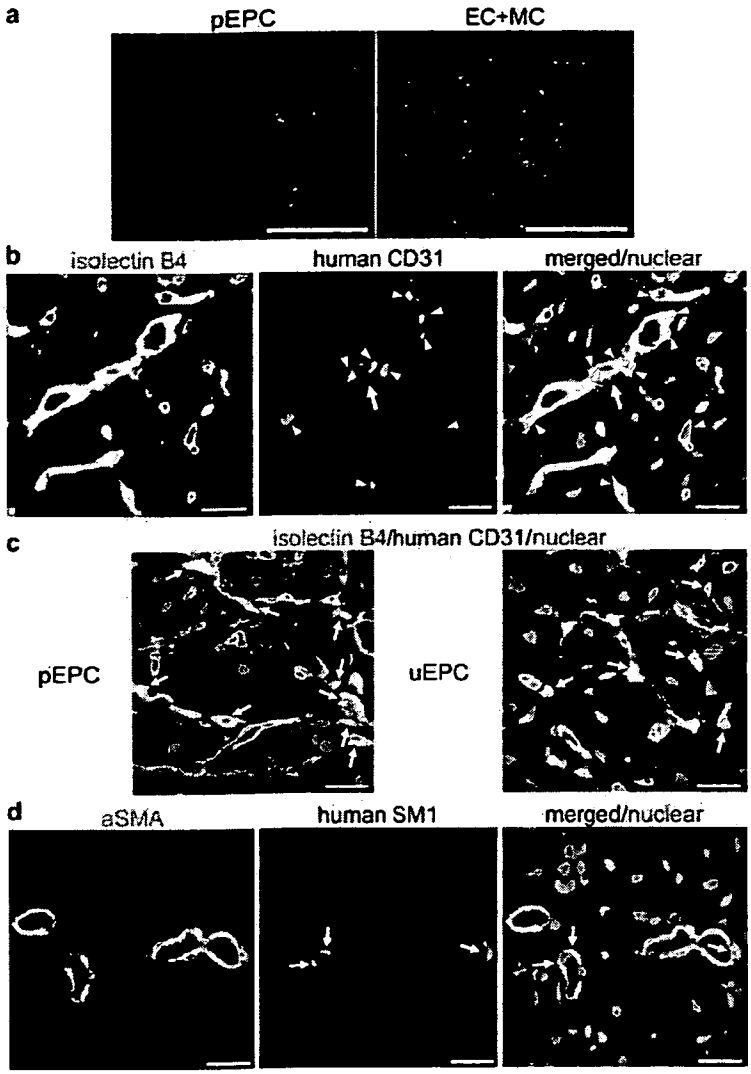

Figure 5. Incorporated human VPC-derived vascular cells at the sites of vascular regeneration. a) Transplanted CM-DiI (red) labeled pEPC or VPC-derived vascular cells in ischemic hindlimbs at day 7 were detected by the fluorescence stereomicroscope. Scale bar: 500 μm. b, c) Immunostaining of frozen sections harvested from ischemic limb tissues at day 14. Fluorescence staining of GSL I-isolectin B4 (green) and human CD31 (blue) with nuclear staining (red) in human VPC-derived EC+MC (b), pEPC, and uEPC (c) transplanted mice. Scale bar: 20 μm. d) Immunostaining of αSMA (green)/human SM1 (blue) with nuclear staining (red) in human VPC-derived EC+MC-transplanted mice at day 14. Scale bar: 20 μm.
doi:10.1371/journal.pone.0001666.g005

stage compared to hAoSMC, and thus, MC could be incorporated into the site of neovascularization.

Recently, Ferreira et al. reported that transplantation of human ES cells-derived EC into nude mice using Matrigel as scaffold contributed for the formation of blood vessels [11]. However, they did not show the direct integration of transplanted human ES cells-derived EC into host blood vessels. Judging from the double staining using intravenously injected isolectin B_4 and anti-human specific CD31 antibody, we found that the transplanted human VPC-derived EC incorporated into host circulating vessels. These transplanted EC could solely form de novo capillaries. In addition, by the double immunostaining of human SM1 and αSMA, we confirmed that transplanted human VPC-derived MC was also incorporated into host vessel walls. Therefore, transplanted human VPC-derived EC and MC structurally contributed to form new vessels in the process of vascular regeneration.

Interaction between EC and MC is essential for vascular development and maintenance of vascular stability [12,13]. Compared to only EC or MC-transplanted mice, the mice transplanted with the combined transplantation of EC and MC showed significant improvement after the induction of ischemic hindlimb. At day 42, the blood flow in the EC+MC group was significantly higher compared to only the EC or MC-transplanted groups. Not only mouse and/or human CD31 but also αSMA positive capillary density at day 42 significantly increased in the EC+MC group. We also found that the density of αSMA positive arterioles also significantly increased in the EC+MC group. These results indicated that combined transplantation of human VPC-derived EC and MC could synergistically contribute to vascular

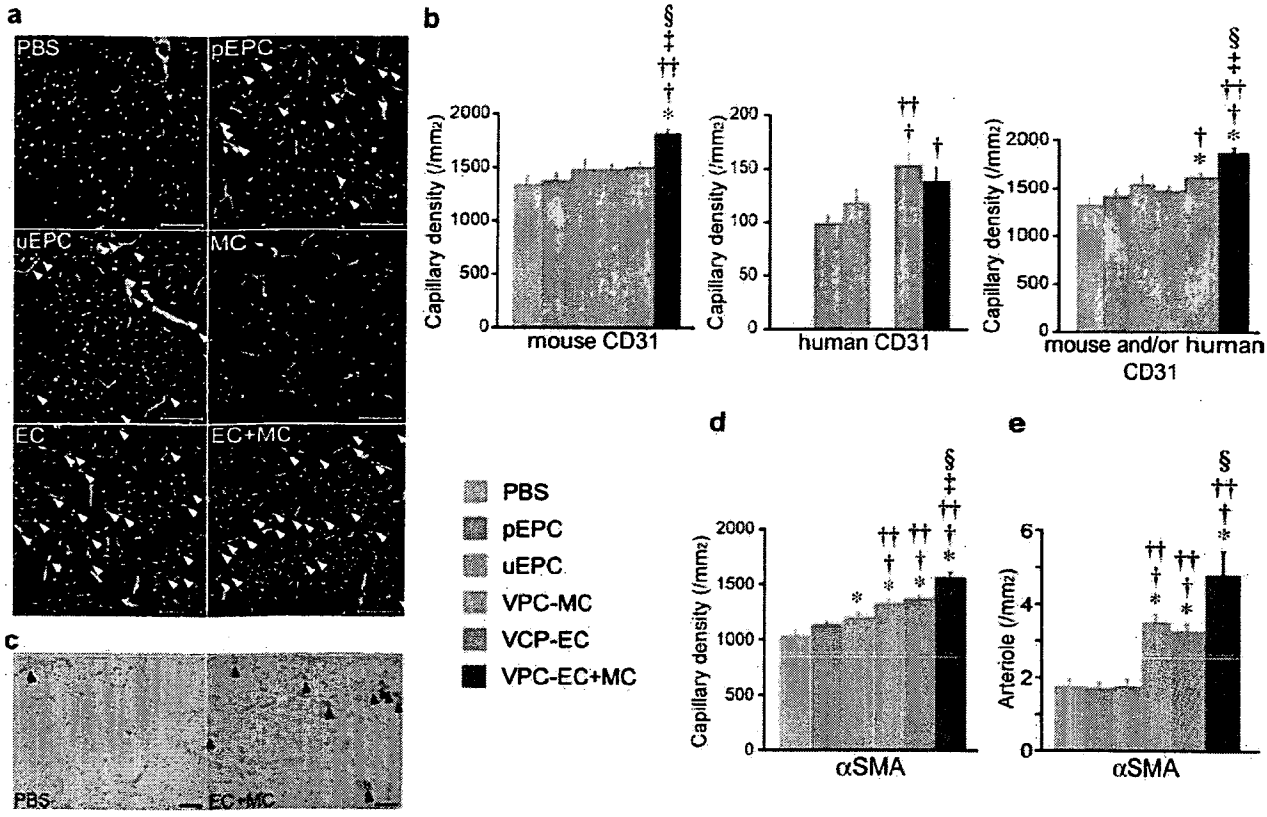

Figure 6. Immunohistochemical analysis of human VPC-derived vascular cells-transplanted murine hindlimb tissues. a) Representative fluorescent photographs of ischemic hindlimb stained for human (red) and mouse (green) CD31 at day 42. Overlapped-stained capillaries are shown in arrowhead. Scale bar: 100 μm. b) Quantitative analysis of the endothelial cell marker positive capillary density in ischemic hindlimbs at day 42. c) Representative αSMA immunostaining (brown) of ischemic hindlimbs at day 42. Scale bar. 100 μm. d) Quantitative analysis of αSMA positive capillary density in ischemic hindlimbs at day 42. e) Quantitative analysis of αSMA positive arterioles (black arrowhead) at day 42. *$P<0.05$ vs. control, †$P<0.05$ vs. pEPC, ††$P<0.05$ vs. uEPC, ‡$P<0.05$ vs. MC, §$P<0.05$ vs. EC.
doi:10.1371/journal.pone.0001666.g006

regeneration, and these MC could make mature blood vessels with adequate MC coating.

VEGFR2 is one of the most specific markers involved in the earliest stage of vascular endothelial and hematopoietic differentiation [14]. Recent reports suggest that VEGFR2$^+$ mesodermal progenitor cells also contribute muscle lineages including vascular smooth, skeletal, and cardiac muscles [1,15]. This evidence indicates the possibility that human VPC-derived MC, which were expanded from VEGFR2$^+$TRA1$^-$VE-cadherin$^-$ cells, might contain skeletal or cardiac muscle cells. However, 40-cycle RT-PCR was confirmed negative for skeletal and cardiac specific markers in expanded human VPC-derived MC. We cultured VPC-derived MC on dishes coated with collagen type IV, which is the major component of basement membrane. Previous reports described that basement membrane played an essential role in endothelial and smooth muscle cell differentiation [16]. Recently, Xiao et al. demonstrated that pretreatment of mouse ES cells with antibodies against collagen IV significantly inhibited smooth muscle cell differentiation [17]. They also demonstrated PDGF receptor-β signaling pathway plays a crucial role in ES cell-derived smooth muscle cell differentiation using PDGF receptor-β siRNA knockdown studies. Therefore, we suspected that, under the presence of collagen type IV and PDGF-BB, our human VPC-derived VE-cadherin negative cells could only differentiate to MC.

Human VPC-derived EC+MC-transplanted KSN nude mice showed considerable blood flow recovery, which led to more than 1.2 in the perfusion ratio of ischemic/non-ischemic limb. When we transplanted human VPC-derived vascular cells to immunosuppressed C57BL/6 mice, the perfusion ratio elevated to nearly 1 (data not shown). Therefore, the tendency of the blood flow recovery in C57BL/6 mice was consistent with the data of KSN nude mice, the absolute value of blood flow ratio after hindlimb ligation was different. Because both KSN nude and C57BL/6 mice received the same procedure for hindlimb ischemia, the degree of perfusion recovery after induction of hindlimb ischemia between these mice might reflect their difference in genetic background for angiogenesis, as reported by Fukino et al [18]. They demonstrated that the VEGF and VEGFR1/2 expression in response to ischemia was impaired in BALB/c mice, compared to other mouse strains (i.e, C57BL/6J or C3H/He mice). These results indicate that, because of the difference in genetic background, spontaneous collateral formation might be accelerated in our KSN nude mice compared to other strain mice.

In transplantation experiments, the number of mouse and/or human CD31 and mouse CD31-positive capillary density in the EC group was 1601.4±51.4/mm^2 and 1470.1±41.6/mm2, respectively. This difference in capillary density (1601.4–1470.1 = 131.3) was consistent with the number of human CD31-positive capillary density (149.9±12.3/mm^2). However,

compared to the EC group, the EC+MC group showed significant augmentation in mouse and/or human CD31 positive capillary density without the increase of human CD31 positive capillary density. One possible reason for this discrepancy is paracrine effects of transplanted human VPC-derived vascular cells might accelerate angiogenesis in ischemic tissues. We demonstrated that cultured human VPC-derived vascular cells expressed several angiogenic factors including VEGF, bFGF, HGF and PDGF-BB, and the release of VEGF from human VPC-derived vascular cells was significantly upregulated after transplantation (data not shown) [4]. Therefore, in addition to the structural contribution of transplanted human VPC-derived vascular cells into the host vascular network, the paracrine effects of these cells might enhance vascular regeneration in tissue ischemia.

Several reports described the contribution of pEPC or uEPC to neovascularization in tissue ischemia [6,7]. However, it has not been clearly demonstrated whether transplanted EPC augment neovascularization through differentiation and proliferation into mature EC or indirectly through paracrine stimulation of resident EC proliferation. Rehamn et al. demonstrated that the majority of pEPC, which were positive for acLDL and ulex-lectin, expressed monocyte/macrophage markers, and only a minority cell fraction expressed the specific endothelial or stem/progenitor markers [8]. They also demonstrated that pEPC did not proliferate, but released several potent angiogenic growth factors. In this study, we confirmed that a low percentage of cultured pEPC and uEPC expressed endothelial makers. A considerable number of pEPC or uEPC were localized inside the capillary lumen, not in the vessel wall. In addition, we found that VEGF mRNA expression in transplanted EPC was significantly higher compared with before transplantation (data not shown). These results suggest that the majority of EPC might have little ability to proliferate or differentiate to endothelial linage, and their angiogenic effects could be attributed to angiogenic factors secreted from transplanted EPC.

In conclusion, we have shown that human VPC-derived cells could effectively differentiate and be expanded to EC and MC. Combined transplantation of these "immature" VPC-derived vascular cells, unlike "mature" somatic EC and MC, augmented reparative neovascularization and contributed to make newly formed vessels in the murine hindlimb ischemia model far more effectively compared to EPC transplantation. Thus, human ES cells-derived EC and MC can be used as the new promising cell source for therapeutic vascular regeneration in patients with tissue ischemia in order to realize a novel combined stem cell therapy.

Materials and Methods

Differentiation of Human VPC-derived EC and MC

Maintenance of human ES cell line (HES3) was as previously described [19]. To induce VPC, undifferentiated ES cells were cultured on an OP9 feeder cell line as reported [3,4]. To obtain human VPC-derived EC, VEGFR2$^+$TRA1$^-$VE-cadherin$^+$ cells were sorted by fluorescence activated cell sorter (FACSAria; Becton Dickinson, Bedford, MA) at day 10 of differentiation, and cultured on type IV collagen-coated dishes (Becton Dickinson) in the presence of 10% FCS and 50ng/ml VEGF (human VEGF165, Peprotech Inc, Rocky Hill, NJ). After 6 passages of these cells, we re-sorted VE-cadherin$^+$ cells for transplantation of human VPC-derived EC. To expand human VPC-derived MC, sorted VEGFR2$^+$TRA1$^-$VE-cadherin$^-$ cells derived from VPC at day 8 were re-cultured on type IV collagen-coated dishes with 1% FCS and 20ng/ml human PDGF-BB (Peprotech Inc). We transplanted these human VPC-derived MC after 6 passages.

Preparation of Human EPC

Peripheral MNC-derived EPC (pEPC) were obtained from healthy volunteer, as previously described [6]. To confirm EPC phenotype, cells were detached with cell dissociation buffer (Invitrogen, Carlsbad, CA) and incubated with DiI-labeled acLDL (Invitrogen) and FITC-labeled Ulex europaeus agglutinin I (ulex-lectin) (Sigma-Aldrich, St. Louis, MO) for 1 hour. These cells were analyzed by FACSAria to be confirmed as EPC [6,8].

Umbilical cord blood-derived CD34$^+$ EPC (uEPC) were isolated from human umbilical cord blood, which were obtained from Cell Bank, RIKEN BioResource Center (Tukuba, Japan). CD34$^+$ cells were separated by a magnetic bead separation method using autoMACS system with direct CD34$^+$ progenitor cell isolation kit (Miltenyi Biotec GmbH, Gladbach, Germany) [7]. Protocols for using human umbilical cord blood were approved by the Ethics Committee of Kyoto University Graduate School of Medicine.

Characterization of VPC-derived Vascular Cells and EPC

To evaluate the surface marker phenotype of VPC-derived vascular cells and EPC, these cells were detached by cell dissociation buffer with or without collagenase (Wako Pure Chemical Industries, Osaka, Japan) and labeled for 15 minutes at 4°C with various fluorescence-conjugated monoclonal antibodies (Table 1) [20]. Cells were washed and analyzed on FACSAria flow cytometer with ≥30,000 events stored.

For the staining of cultured VPC-derived vascular cells on dishes, cells were stained with anti-human CD31 (WM59) (Becton Dickinson) antibody and several smooth muscle specific markers, as shown in Table 2. Cultured hAoSMC (Cambrex, East Rutherford, NJ) were used to obtain positive control staining.

For RT-PCR analysis, total RNA was prepared with RNeasy Mini Kit (QIAGEN Inc., Valencia, CA), and RT-PCR was performed by TaKaRa One Step RNA PCR Kit (TaKaRa Bio Inc., Otsu, Japan). Total RNA from human heart and skeletal muscle were purchased from Clontech (Mountain View, CA). Primers are listed in Table 3 [21–23].

Hindlimb Ischemia Model and Cell Transplantation

After 8-week-old male KSN/Slc nude mice (Japan SLC, Shizuoka, Japan) were anesthetized with pentobarbital (80mg/kg, i.p.), the right femoral vein was ligated. To transplant vascular cells intra-arterially, we injected these cells in 100 μl PBS into the right femoral artery. Immediately after the cell injection, the right femoral artery and vein were ligated and excised [24]. Animal procedures were performed according to Kyoto University standards for animal care.

Assessment of Transplanted Animals

The measurement of hindlimb blood flow was performed with a LDPI analyzer (Moor Instruments, Devon, United Kingdom), as previously described [24].

At arbitrary time points, biotin conjugated Griffonia simplicifolia lectin (GSL) I-isolectin B_4 (Vector Laboratories, Burlingame, CA) in 100 μl PBS was injected into the portal vein 15 minutes before sacrifice. Cryostat sections (10 μm thick) of the ischemic lower legs were stained with anti-mouse/human CD31 (clone WM59/Mec13.3) (Becton Dickinson) or anti-αSMA/human SM1 (clone 1A4/3F8) (DakoCytomation, Glostrup, Denmark/Yamasa Co., Tokyo, Japan) antibodies. For biotinylated isolectin B_4 staining to detect circulating vessels, sections were incubated with streptoavidin conjugated Alexa Fluor dye (Invitrogen).

Capillary densities were examined by counting the number of capillaries stained with anti-human and/or mouse CD31 or anti-

Table 1. Fluorescence-conjugated monoclonal antibodies used for FACS analysis

Antibody	Specificity	Clone	Conjugated fluorescence	Supplier
VEGF-R2	Endothelial cells	KM1998	Alexa Fluor 647	A generous gift of Prof. M. Shibuya, Tokyo University (Ref.20)
VE-cadherin	Endothelial cells	55-7H1	FITC or PE	Becton Dickinson, Bedford, MA
von Willebrand Factor (vWF)	Endothelial cells	2F2-A9	Alexa Fluor 488	Becton Dickinson, Bedford, MA
CD31 (PECAM1)	Endothelial cells or Monocytes	WM59	Alexa Fluor 488	eBioscience, San Diego, CA
CD105 (Endoglin)	Endothelial cells or Monocytes	266	Alexa Fluor 647	Becton Dickinson, Bedford, MA
CD11b (Mac1)	Monocytes	ICRF44	PE	eBioscience, San Diego, CA
CD11c	Monocytes	B-ly6	FITC	Becton Dickinson, Bedford, MA
CD14	Monocytes	M5E2	APC	Becton Dickinson, Bedford, MA
CD45	Panleukocytes	H30	PE	Becton Dickinson, Bedford, MA
CD54 (ICAM-1)	Panleukocytes	581	PE	Becton Dickinson, Bedford, MA
AC133	Stem/Progenitor cells	AC133	PE	Miltenyi Biotec GmbH, Bergisch Gladbach, Germany
c-kit	Stem/Progenitor cells	YB5.B8	APC	Becton Dickinson, Bedford, MA
CD34	Stem/Progenitor cells	581	FITC	Becton Dickinson, Bedford, MA

doi:10.1371/journal.pone.0001666.t001

Table 2. Smooth muscle specific antibodies used for analysis

Antibody	Specificity	Clone	Supplier
Alpha smooth muscle actin (αSMA)	Human & mouse	1A4	DakoCytomation Denmark A/S, Glostrup, Denmark Sigma-Aldrich, St. Louis, MO
Calponin	Human	CALP	DakoCytomation Denmark A/S, Glostrup, Denmark
Smooth muscle myosin heavy chain 1 (SM1)	Human	3FB	Yamasa Co., Tokyo, Japan
Smooth muscle myosin heavy chain 2 (SM2)	Human & mouse	1G12	Yamasa Co., Tokyo, Japan

doi:10.1371/journal.pone.0001666.t002

Table 3. Primers for reverse transcription-polymerase chain reaction

Gene		Sequence	Length (bp)
Calponin[1]	Sense	5'-CTTCATGGACGGCCTCAAAGA-3'	713
	Antisense	5'-GTAGTTGTGTGCGTGGTGGTT-3'	
Smooth muscle myosin heavy chain 1 (SM1) and 2 (SM2)[1, 2]	Sense	5'-ATGAGGCCACGGAGAGCAACGA-3'	178 (SM1)
	Antisense	5'-CCATTGAAGTCTGCGTCTCGA-3'	217 (SM2)
h-caldesmon[1]	Sense	5'-AGACAAGGAAAGAGCTGAGGCA-3'	395
	Antisense	5'-GCTGCTTGTTACGTTTCTGCTC-3'	
Glyceraldehyde-3-phosphate dehydrogenase (GAPDH)[1]	Sense	5'-ACCACAGTCCATGCCATCAC-3'	452
	Antisense	5'-TCCACCACCCTGTTGCTGTA-3'	
Myogenin[3]	Sense	5'-GTGGGCGTGTAAGGTGTGTA-3'	141
	Antisense	5'-TGGTTGGGGTTGAGCAGGGT-3'	
MyoD[3]	Sense	5'-CCAAATGTAGCAGGTGTAAC-3'	142
	Antisense	5'-AGAGATAAATACAGCCCCAG-3'	
Cardiac troponin T (cTnT)[4]	Sense	5'-GGCAGCGGAAGAGGATGCTGAA-3'	150
	Antisense	5'-GAGGCACCAAGTTGGGCATGAACGA-3'	
Cardiac troponin I (cTnI)[4]	Sense	5'-CCCTGCACCAGCCCCAATCAGA-3'	250
	Antisense	5'-CGAAGCCCAGCCCGGTCAACT-3'	

[1]Ref. 21.
[2]We used a single pair of PCR primers that cover the sequence specific to SM2, because these two isoforms are produced from a single gene by alternative splicing.
[3]Ref. 22.
[4]Ref. 23.
doi:10.1371/journal.pone.0001666.t003

αSMA antibodies. Twenty (for CD31) or ten (for αSMA) random fields on two different sections (approximately 3mm apart) from each mouse were photographed and analyzed by NIH image as previously described [24].

Statistical Analysis

Results are presented as means±S.E.M. The serial changes of the hindlimb blood flow were assessed by repeated measures ANOVA, followed by Bonferoni's multiple comparison test. Comparisons among groups were tested by one-way ANOVA followed by Bonferoni's multiple comparison test. A P value <0.05 was considered significant.

References

1. Yamashita J, Itoh H, Hirashima M, Ogawa M, Nishikawa S, et al. (2000) Flk1-positive cells derived from embryonic stem cells serve as vascular progenitors. Nature 408: 92–96.
2. Yurugi-Kobayashi T, Itoh H, Yamashita J, Yamahara K, Hirai H, et al. (2003) Effective contribution of transplanted vascular progenitor cells derived from embryonic stem cells to adult neovascularization in proper differentiation stage. Blood 101: 2675–2678.
3. Sone M, Itoh H, Yamashita J, Yurugi-Kobayashi T, Suzuki Y, et al. (2003) Different differentiation kinetics of vascular progenitor cells in primate and mouse embryonic stem cells. Circulation 107: 2085–2088.
4. Sone M, Itoh H, Yamahara K, Yamashita JK, Yurugi-Kobayashi T, et al. (2007) Pathway for differentiation of human embryonic stem cells to vascular cell components and their potential for vascular regeneration. Arterioscler Thromb Vasc Biol 27: 2127–2134.
5. Asahara T, Murohara T, Sullivan A, Silver M, van der Zee R, et al. (1997) Isolation of putative progenitor endothelial cells for angiogenesis. Science 275: 964–967.
6. Kalka C, Masuda H, Takahashi T, Kalka-Moll WM, Silver M, et al. (2000) Transplantation of ex vivo expanded endothelial progenitor cells for therapeutic neovascularization. Proc Natl Acad Sci U S A 97: 3422–3427.
7. Murohara T, Ikeda H, Duan J, Shintani S, Sasaki K, et al. (2000) Transplanted cord blood-derived endothelial precursor cells augment postnatal neovascularization. J Clin Invest 105: 1527–1536.
8. Rehman J, Li J, Orschell CM, March KL (2003) Peripheral blood "endothelial progenitor cells" are derived from monocyte/macrophages and secrete angiogenic growth factors. Circulation 107: 1164–1169.
9. Fina L, Molgaard HV, Robertson D, Bradley NJ, Monaghan P, et al. (1990) Expression of the CD34 gene in vascular endothelial cells. Blood 75: 2417–2426.
10. Frid MG, Shekhonin BV, Koteliansky VE, Glukhova MA (1992) Phenotypic changes of human smooth muscle cells during development: late expression of heavy caldesmon and calponin. Dev Biol 153: 185–193.
11. Ferreira LS, Gerecht S, Shieh HF, Watson N, Rupnick MA, et al. (2007) Vascular progenitor cells isolated from human embryonic stem cells give rise to endothelial and smooth muscle like cells and form vascular networks in vivo. Circ Res 101: 286–294.
12. Chan-Ling T, Page MP, Gardiner T, Baxter L, Rosinova E, et al. (2004) Desmin ensheathment ratio as an indicator of vessel stability: evidence in normal development and in retinopathy of prematurity. Am J Pathol 165: 1301–1313.
13. Hughes S, Chan-Ling T (2004) Characterization of smooth muscle cell and pericyte differentiation in the rat retina in vivo. Invest Ophthalmol Vis Sci 45: 2795–2806.
14. Nishikawa SI, Nishikawa S, Hirashima M, Matsuyoshi N, Kodama H (1998) Progressive lineage analysis by cell sorting and culture identifies FLK1+VE-cadherin+ cells at a diverging point of endothelial and hemopoietic lineages. Development 125: 1747–1757.
15. Motoike T, Markham DW, Rossant J, Sato TN (2003) Evidence for novel fate of Flk1+ progenitor: contribution to muscle lineage. Genesis 35: 153–159.
16. Sakata N, Kawamura K, Takebayashi S (1990) Effects of collagen matrix on proliferation and differentiation of vascular smooth muscle cells in vitro. Exp Mol Pathol 52: 179–191.
17. Xiao Q, Zeng L, Zhang Z, Hu Y, Xu Q (2007) Stem cell-derived Sca-1+ progenitors differentiate into smooth muscle cells, which is mediated by collagen IV-integrin alpha1/beta1/alphav and PDGF receptor pathways. Am J Physiol Cell Physiol 292: C342–352.
18. Fukino K, Sata M, Seko Y, Hirata Y, Nagai R (2003) Genetic background influences therapeutic effectiveness of VEGF. Biochem Biophys Res Commun 310: 143–147.
19. Reubinoff BE, Pera MF, Fong CY, Trounson A, Bongso A (2000) Embryonic stem cell lines from human blastocysts: somatic differentiation in vitro. Nat Biotechnol 18: 399–404.
20. Sawano A, Iwai S, Sakurai Y, Ito M, Shitara K, et al. (2001) Flt-1, vascular endothelial growth factor receptor 1, is a novel cell surface marker for the lineage of monocyte-macrophages in humans. Blood 97: 785–791.
21. Miwa Y, Sasaguri T, Inoue H, Taba Y, Ishida A, et al. (2000) 15-Deoxy-Delta(12,14)-prostaglandin J(2) induces G(1) arrest and differentiation marker expression in vascular smooth muscle cells. Mol Pharmacol 58: 837–844.
22. Kato H, Ohta S, Koshida S, Narita T, Taga T, et al. (2003) Expression of pericyte, mesangium and muscle markers in malignant rhabdoid tumor cell lines: differentiation-induction using 5-azacytidine. Cancer Sci 94: 1059–1065.
23. Kehat I, Kenyagin-Karsenti D, Snir M, Segev H, Amit M, et al. (2001) Human embryonic stem cells can differentiate into myocytes with structural and functional properties of cardiomyocytes. J Clin Invest 108: 407–414.
24. Yamahara K, Itoh H, Chun TH, Ogawa Y, Yamashita J, et al. (2003) Significance and therapeutic potential of the natriuretic peptides/cGMP/cGMP-dependent protein kinase pathway in vascular regeneration. Proc Natl Acad Sci U S A 100: 3404–3409.

Acknowledgments

The human ES cells (HES3) were provided by ES Cell International Pre Ltd., Singapore.

Author Contributions

Conceived and designed the experiments: KY HI KN MS JY TY TC KH DT KM KP NO NS NT YF. Performed the experiments: KY MS KH. Analyzed the data: KY. Wrote the paper: KY HI.

Selective Impairment of Working Memory in a Mouse Model of Chronic Cerebral Hypoperfusion

Masunari Shibata, MD; Nobuyuki Yamasaki, MD; Tsuyoshi Miyakawa, PhD; Rajesh N. Kalaria, PhD, FRCPath; Youshi Fujita, MD; Ryo Ohtani, MD; Masafumi Ihara, MD; Ryosuke Takahashi, MD; Hidekazu Tomimoto, MD

Background and Purpose—We recently designed a mouse model of chronic cerebral hypoperfusion, in which the cerebral white matter is damaged without significant gray matter lesions. The behavioral characteristics of these mice were studied using a test battery for neurological and cognitive functions.

Methods—Adult C57Bl/6 male mice were subjected to either sham-operation or bilateral common carotid artery stenosis (BCAS) using microcoils with an internal diameter of 0.18 mm. At 30 days after BCAS, 70 animals were divided into 3 groups and subjected to behavioral test batteries. The first group underwent comprehensive behavioral test, including the neurological screen, prepulse inhibition, hot plate, open field, light/dark transition, Porsolt forced swim and contextual and cued fear conditioning (BCAS n=13; sham-operated n=11). The second group was for the working memory task of the 8-arm radial maze test (BCAS n=12; sham-operated n=10), and the third for the reference memory task of the 8-arm radial maze test (BCAS n=13; sham-operated n=11). Another batch of animals were examined for histological changes (BCAS n=11; sham-operated n=12).

Results—The white matter including the corpus callosum was consistently found to be rarefied without clear ischemic lesions in the hippocampus. No apparent differences were observed in the comprehensive test batteries between the control and BCAS mice. However, in the working memory tasks tested with the 8-arm radial maze, the BCAS mice made significantly more errors than the control mice ($P<0.0001$). Again, there were no detectable differences in the reference memory tasks between the groups.

Conclusions—At 30 days after BCAS, working memory deficits as well as white matter changes were apparent in the mice. Working memory deficit was attributable to damage of the frontal-subcortical circuits, suggesting the BCAS model is useful to evaluate the substrates of subcortical vascular dementia. (***Stroke.* 2007;38:2826-2832.)**

Key Words: behavioral neurology ■ cerebral blood flow ■ hippocampus ■ leukoaraiosis ■ memory ■ vascular dementia ■ white matter disease

Cerebral blood flow (CBF) is decreased in patients with vascular dementia. Subcortical vascular dementia, the major subtype of vascular dementia, is featured by small vessel disease involving white matter (WM) changes and lacunar infarctions. Arteriosclerosis may induce these WM lesions after longstanding cerebral hypoperfusion.[1] In support for this hypothesis, hypoxia-inducible factor-1 is expressed in cerebrovascular WM lesions.[2] In addition, WM lesions are observed in rodent models of chronic cerebral hypoperfusion, in which the bilateral carotid arteries are stenosed or ligated,[3–7] and stroke-prone spontaneously hypertensive rats which have small vessel pathology.[8] Such WM lesions are suggested to contribute to frontal hypometabolism and executive dysfunction.[9,10]

We recently designed a mouse model of chronic cerebral hypoperfusion[11] by placing microcoils bilaterally on the common carotid arteries. These mice invariably exhibited WM changes and have several advantages over other models of chronic cerebral hypoperfusion in rats and gerbils.[3–5,12–14] First, genetically modulated mice produced to model various diseases can be used.[15] Second, the visual pathway is preserved as compared with the rat model, because blood flow in the common carotid arteries albeit reduced is maintained. Third, the cerebral WM is selectively damaged, yet sparing the gray matter such as the hippocampus if the degree of stenosis is appropriately controlled by adjusting the internal diameter of the microcoils.[11]

Received April 4, 2007; accepted April 18, 2007.

From the Department of Neurology (M.S., Y.F., R.O., M.I., R.T., H.T.), Graduate School of Medicine, and Horizontal Brain Research Organization (N.Y., T.M.), Kyoto University, Sakyo-ku, Kyoto, Japan; and the Institute for Health and Ageing (R.N.K.), University of Newcastle upon Tyne, Newcastle General Hospital, Newcastle-upon-Tyne, UK.

Correspondence to Hidekazu Tomimoto, MD, Department of Neurology, Graduate School of Medicine, Kyoto University, Sakyo-ku, Kyoto 606-8507, Japan. E-mail tomimoto@kuhp.kyoto-u.ac.jp

Stroke **is available at http://stroke.ahajournals.org** **DOI: 10.1161/STROKEAHA.107.490151**

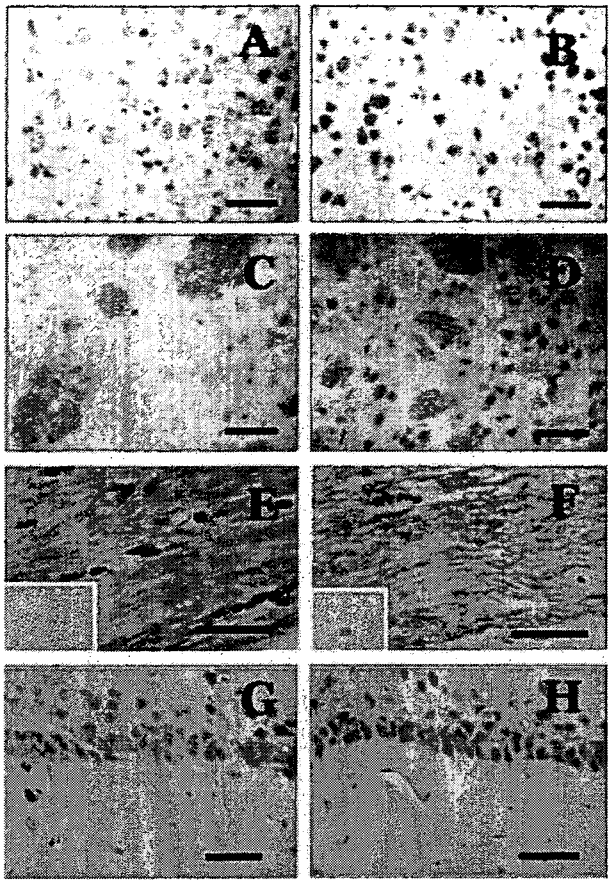

Figure 1. Photomicrographs of Klüver-Barrera staining (A through H) and TUNEL (insets in E and F) in the cerebral cortex (A and B), caudoputamen (C and D), corpus callosum (E and F) and hippocampus (G and H). The left column (A, C, E, and G) indicates the brain from a sham-operated mouse and the right column (B, D, F, and H) indicates a brain after BCAS for 30 days. Note marked vacuoles (F), and intact pyramidal neurons (H) after BCAS. Bars indicate 100 μm (C through F).

In the present study, we used various paradigms to test behavior including working and reference memories in this bilateral carotid artery stenosis (BCAS) mice model of chronic cerebral hypoperfusion. The BCAS model would be useful to explore behavioral substrates of the frontal-subcortical circuit deficits apparent in subcortical vascular dementia.

Materials and Methods

Animals and Experimental Design

Male C57Bl/6 mice (10 to 12 weeks old, 24 to 29 g; Shizuoka laboratory animal center, Hamamatsu) were anesthetized with sodium pentobarbital. Through a midline cervical incision, both common carotid arteries were exposed. A microcoil with a diameter of 0.18 mm was applied to the bilateral common carotid artery, maintaining the rectal temperature between 36.5°C and 37.5°C. Those in the control group were sham-operated, which involved bilateral exposure of the common carotid arteries. The animals were kept in cages for 30 days with food and water ad libitum.

Twenty four mice were examined for histological changes. After BCAS, CBF was measured by laser-Doppler flowmetry at 1, 7 and 30 days, as described previously.[11] These mice were deeply anesthetized with sodium pentobarbital and were perfused transcardially with 0.01 mol/L phosphate-buffered saline (PBS) and then with a fixative containing 4% paraformaldehyde and 0.2% picric acid in 0.1 mol/L phosphate buffer (PB, pH 7.4). The brains were postfixed in 4% paraformaldehyde in 0.1 mol/L PB, and were stored in 20% sucrose in 0.1 mol/L PB (pH 7.4). The brains were then embedded in paraffin and sliced into 6 μm-thick coronal sections. Sequential sections from every 50 to 100 sections were stained with Klüver-Barrera (KB) and hematoxylin and eosin (H&E) stains. TUNEL staining was done using Apoptag in situ kit obtained from Oncor. The WM changes were evaluated specifically in 4 regions: the optic tract, internal capsule, fiber bundles of the caudoputamen, and corpus callosum. In the coronal plane 0.15 mm anterior to the bregma, the areas of right hemisphere and ventricular space 30 days after the operation were digitized using the NIH image analyzer program, and used as an index of brain atrophy.

Another 70 animals, which were 14 to 16 weeks old were divided into 3 groups and examined 30 days after the operation. The first group of the mice was subjected to a comprehensive behavioral test battery.[16,17] The battery included the neurological screen, light/dark transition, open field, hot plate, prepulse inhibition and Porsolt forced swim, contextual and cued fear conditioning, which were conducted in this sequence, with each test separated at least by 1 day (BCAS mice, n=13; sham-operated, n=11). The second group was tested for the working memory task of the 8-arm radial maze (BCAS mice, n=12; sham-operated, n=10), and the third group for the reference memory task (BCAS mice, n=13; sham-operated, n=11).

The mice were housed in a room with a 12-hour light/dark cycle (lights on at 7:00 AM) with access to food and water ad libitum. All procedures were performed according to the guidelines of the Animal Use and Care Committee of Kyoto University.

Neurological Screen

A neurological screen was conducted as previously described.[17] The ear twitch, whisker touch and righting reflexes were evaluated.

Startle Response/Prepulse Inhibition Tests

A startle reflex measurement system was used (O'Hara & Co). The test session began by placing a mouse in a plexiglasss cylinder for 10 minutes. The duration of white noise as the startle stimulus was 40 ms for all trial types. The startle response was recorded for 140 ms (measuring the response every 1 ms) starting with the onset of the prepulse stimulus. The peak startle amplitude recorded during the 140-ms sampling window was used as the dependent variable. A test session consisted of 6 trial types (ie, 2 types for startle stimulus only trials, and 4 types for prepulse inhibition trials). The intensity of startle stimulus was 110 or 120 dB. The prepulse sound was presented 100 ms before the startle stimulus, and its intensity was 74 or 78 dB. Four combinations of prepulse and startle stimuli were used (74/110, 78/110, 74/120, and 78/120). Six blocks of the 6 trial types were presented in pseudorandom order such that each trial type was presented once within a block. The average intertrial interval was 15 s (range: 10 to 20 s).

Hot Plate Test

The hotplate test for nociception was used to evaluate sensitivity to a thermal stimulus. Mice were placed on a 55.0 (±0.3)°C hot plate (Columbus Instruments), and latency to the first hind-paw response (a foot shake or a paw lick) was recorded.

Motor Function Tests

Motor coordination and balance were tested with the rotarod test, and neuromuscular strength was tested with wire hang test and grip strength test.[17] In the wire hang test, the mouse was placed on a wire cage lid apparatus (O'hara & Co) to assess balance and grip strength. The mouse was placed on a wire mesh, which was then inverted, and latency to fall was recorded. A grip strength meter (O'hara & Co) was used to assess forelimb grip strength, when mice were pulled back. The rotarod test was performed by placing a mouse on a rotating drum (UGO Basile Accelerating Rotarod), and the time to maintain its balance on the rod was measured. The speed of the rotarod was accelerated from 4 to 40 rpm over a 5-minute period.

Table. General Physical Characteristics and Sensory/Motor Functions of BCAS Mice and Sham-Operated Mice

	BCAS	Sham	*P* Value
Physical characteristics			
Age, wk	14.1	14.1	
Whiskers, % with	100	100	
Fur, % with normal fur	100	100	
Rectal temperature, °C	36.9 (±0.1)	37.0 (±0.1)	$F_{1,22}$=0.495, *P*=0.4893
Sensory motor reflex			
Ear twitch, % with quick response	100	100	
Whisker twitch, % with normal response	100	100	
Righting reflex, % with normal response	100	100	
Acoustic startle response, arbitrary unit			
Stimulus intensity=110 dB	1.2 (±0.1)	1.3 (±0.2)	$F_{1,21}$=0.042, *P*=0.8393
Stimulus intensity=120 dB	1.8 (±0.2)	1.9 (±0.3)	$F_{1,21}$=0.094, *P*=0.762
Prepulse inhibition (%; stimulus=110 dB)			
Prepulse intensity=74 dB	42.2 (±8.0)	22.3 (±6.7)	$F_{1,21}$=3.566, *P*=0.0729
Prepulse intensity=78 dB	61.7 (±6.0)	48.9 (±4.0)	$F_{1,21}$=3.026, *P*=0.0966
Prepulse inhibition (%; stimulus=120 dB)			
Prepulse intensity=74 dB	31.1 (±10.4)	23.6 (±7.0)	$F_{1,21}$=0.342, *P*=0.5651
Prepulse intensity=78 dB	50.7 (±7.6)	44.2 (±5.6)	$F_{1,21}$=0.465, *P*=0.5027
Pain test			
Hot plate test (latency; s)	7.7 (±0.6)	7.6 (±0.6)	$F_{1,22}$=0.003, *P*=0.9548
Motor test			
Wire hang (latency to fall; s)	51.1 (±4.0)	60.0 (±0.0)	$F_{1,22}$=4.108, *P*=0.055
Grip strength (N)	0.83 (±0.04)	0.81 (±0.04)	$F_{1,22}$=0.266, *P*=0.611
Rotarod (latency to fall; s; average of 3 trials)			
Day 1	137 (±13)	167 (±14)	$F_{1,22}$=2.254, *P*=0.1475
Day 2	201 (±17)	226 (±13)	$F_{1,22}$=1.274, *P*=0.2712

Data represent the mean (±SEM; BCAS, n=13; sham, n=11).

Open Field Test

Locomotor activity was measured using an open field test. Each subject was placed in the center of the open field apparatus (40×40×30 cm; Accuscan Instruments). Total distance traveled (in cm), vertical activity (rearing measured by counting the number of photobeam interruptions), time spent in the center, and the beam-break counts for stereotyped behavior (stereotypic counts) were recorded. Data were collected for 120 minutes.

Light/Dark Transition Test

The apparatus used for the light/dark transition test consisted of a cage (21×42×25 cm) divided into 2 chambers, one of which was brightly illuminated (390 lux), and the other was dark (2 lux). Mice were placed into the dark side and allowed to move freely for 10 minutes. The total number of transitions, time spent in each side, first latency to light side, and distance traveled were recorded by Image LD software (see 'Image Analysis').

Porsolt Forced Swim Test

In the Porsolt forced swim test, the apparatus consisted of 4 plexiglass cylinders (20 cm height ×10 cm diameter). The cylinders were filled with water (23°C), up to a height of 7.5 cm. Mice were placed into the cylinders, and their behavior was recorded over a 10-minute test period (day 1, 2). Data acquisition and analysis were performed automatically, using Image PS software (see 'Image Analysis').

Contextual and Cued Fear Conditioning

Each mouse was placed in a test chamber (26×34×33 cm; O'hara & Co) and allowed to explore freely for 2 minutes. A 55-dB white noise, which served as the conditioned stimulus, was presented for 30 s, followed by a mild (2 s, 0.3 mA) footshock, which served as the unconditioned stimulus. Two more conditioned stimulus–unconditioned stimulus pairings were presented with 2-minute interstimulus interval. Context testing was conducted 24 hours after conditioning in the same chamber. Cued testing with altered context was conducted 24 hours after conditioning using a triangular box (35×35×41 cm), which was located in a different room.

Data acquisition, control of stimuli, and data analysis were performed automatically, using Image FZ software (see 'Image Analysis'). Images were captured at 1 frame per second. For each pair of successive frames, the amount of area (pixels) by which the mouse moved was measured. When this area was below a certain threshold (ie, 20 pixels), the behavior was judged as 'freezing'. The optimal threshold (amount of pixels) to judge freezing was determined by adjusting it to the amount of freezing measured by human observation.

Eight-Arm Radial Maze Test

The 8-arm radial maze test was conducted as described previously.[17] Each arm (9×40 cm) radiated from an octagonal central starting platform. Identical food wells with pellet sensors were placed at the distal end of each arm. As the initial pretraining, each mouse was placed in the central starting platform and allowed to explore and to consume food pellets scattered on the whole maze for a 5-minute period. Subsequently, these mice received another pretraining to take a pellet from each food well after being placed at the distal end of each arm. A trial was finished after the subject consumed the pellet. This was repeated 8 times, using 8 different arms, for each mouse.

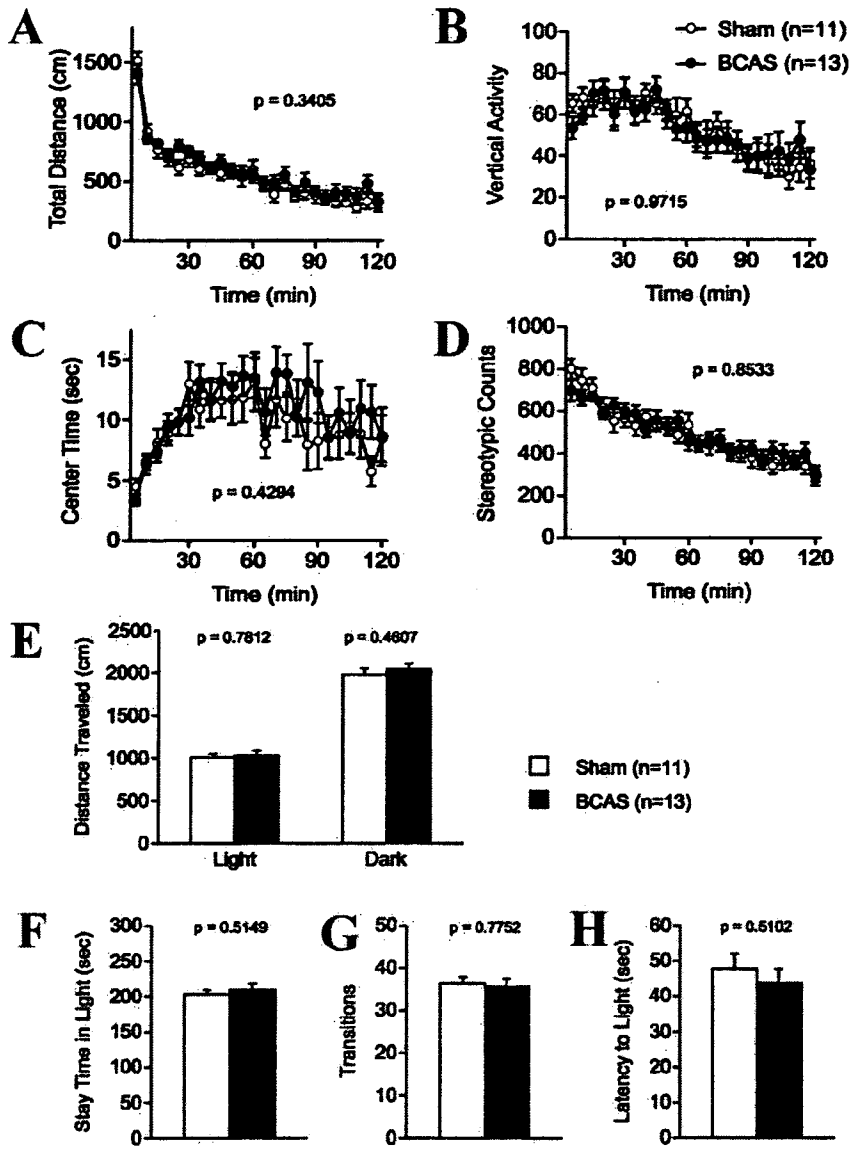

Figure 2. Locomotor activity of the control and BCAS mice in an open field test (A through D). No differences was observed for total distance traveled (group effect, $F_{1,22}=0.949$, $P=0.3405$; A), vertical activity (group effect, $F_{1,22}=0.001$, $P=0.9715$; B), time spent in the center area (group effect, $F_{1,22}=0.648$, $P=0.4294$; C), and the number of stereotypic counts (group effect, $F_{1,22}=0.035$, $P=0.8533$; D). Locomotor activity in the light/dark transition test (E through H). No difference was observed for distance traveled in light (group effect, $F_{1,22}=0.079$, $P=0.7812$) and dark chamber (group effect, $F_{1,22}=0.564$, $P=0.4607$; E), time spent in light (group effect, $F_{1,22}=0.438$, $P=0.5149$; F), number of transitions between the light and dark sides (group effect, $F_{1,22}=0.084$, $P=0.7752$; G), and latency to enter the light side ($F_{1,22}=0.448$, $P=0.5102$; H).

In spatial working memory task of the 8-arm radial maze, all 8 arms were baited with food pellets. Mice were placed on the central platform and allowed to get all 8 pellets within 25 minutes. A trial was terminated immediately after all 8 pellets were consumed or 25 minutes had elapsed. For each trial, choices of arms, latency to get all pellets, distance traveled, number of different arms chosen within the first 8 choices, and the number of revisiting, and omission errors were automatically recorded.

In reference memory task of the 8-arm radial maze, one of the 8 arms was constantly baited by one pellet in a food well and a trial was terminated immediately after one pellet was consumed. Data acquisition, control of guillotine doors, and data analysis were performed by Image RM software (see 'Image Analysis').

Image Analysis and Statistical Analysis

The applications used for the behavioral studies (Image LD, Image OF, Image PS, Image RM, and Image FZ) were based on the public domain National Institutes of Health's Image program.[18] Statistical analysis was conducted using StatView (SAS Institute). Data were analyzed by 2-way ANOVA, or 2-way repeated measures ANOVA, unless noted otherwise. Values in the table and graphs were expressed as mean±SEM.

Results

Histological Findings

All of the mice regained consciousness within a few hours after the operation, but occasionally showed transient ptosis. None of them showed any apparent motor weakness. The CBF values (ratio to the preoperative value) was not changed significantly in the sham-operated mice, but decreased to 72.4±17.3% at day 1, 77.3±15.3% at day 7 and 83.4±13.6% at day 30 after BCAS. The blood pressure measured either at day 1, 7 and 30 days was not different between the BCAS and sham-operated mice. The staining intensity of the myelinated fibers was reduced, and the integrity of the myelin was compromised in the corpus callosum (Figure 1E and 1F), caudoputamen, internal capsule and optic tract, as reported previously.[11] The remaining fibers were disorganized and vacuoles were frequently observed in the neuropil. Atrophy was not found in the optic nerve (photo not shown), although being rarefied slightly. Of the brains examined, there were no

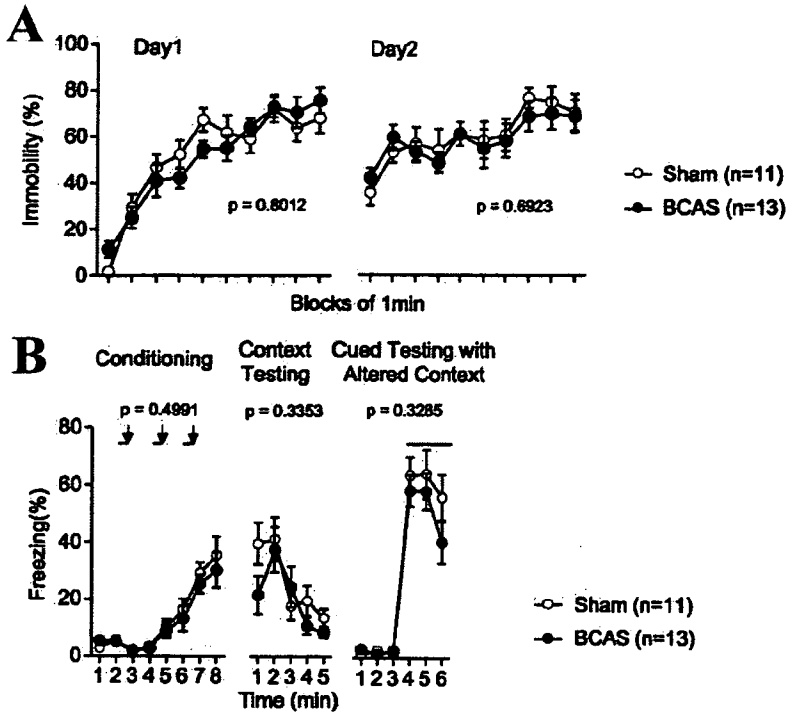

Figure 3. Behavioral despair of mice in the Porsolt forced swim test (A). Mice traveled at day 1 and day 2 (for day1, group effect, $F_{1,22}=0.065$, $P=0.8012$; for day 2, $F_{1,22}=0.161$, $P=0.6923$). Data are given as means (±SEM). Percentage of freezing during conditioning, context testing and cued testing with altered context in control and BCAS mice (B). Data are given as means (±SEM). In the contextual and cued fear conditioning test, there was no significant difference in freezing during conditioning (group effect, $F_{1,22}=0.472$, $P=0.4991$), context testing (group effect, $F_{1,22}=0.970$, $P=0.3353$), and cued testing with altered context (group effect, $F_{1,22}=0.998$, $P=0.3285$) between the groups.

infarctions or hemorrhage in any gray matter regions including the cerebral cortex, caudoputamen and hippocampus (Figure 1A through 1D, 1G, and 1H). There were only a few TUNEL positive cells in the corpus callosum (Figure 1, insets in 1E and 1F), but not in the hippocampus.

The hemispheric area was 20.4±2.7 mm^2 (mean±SEM) for BCAS mice and 20.9±1.4 mm^2 for sham-operated mice. The ventricular space area was 0.51±0.2 mm^2 for BCAS mice and 0.53±0.31 mm^2 for sham-operated mice. For both areas, there were no significant differences between the groups.

Physical Characteristics, Sensory Motor Reflexes, Nociception, Motor Coordination

As shown in the Table, there were no significant differences between BCAS and sham-operated mice in terms of their physical characteristics. Body weight in BCAS and sham-operated mice were 25.7±0.2 and 25.3±0.2, respectively, before operation, 23.8±0.2 and 24.1±0.2 after 3 days, and 27.4±0.3 and 27.0±0.4 after 30 days indicating no significant differences between the groups.

There were also no differences in sensory-motor reflexes (percent with quick response of ear twitch, normal response of whisker twitch and righting reflex, acoustic startle response), sensory-motor gating (prepulse inhibition), nociception (hot plate test), and motor coordination (wire hang and rotarod tests).

Locomotor Activity

There were also no differences between BCAS and sham-operated mice for total distance traveled, vertical activity, time spent in the center area, and the number of stereotypic counts in an open field test (Figure 2A through 2D). In the light /dark transition test (Figure 2E through 2H), there was also no differences between the groups for distance traveled in light and dark chamber, time spent in light, number of transitions between the light and dark sides and latency to enter the light side.

Porsolt Forced Swim Test, and Contextual and Cued Fear Conditioning Test

The ratio of immobility was not different between the groups both at day 1 and day 2 in Porsolt forced swim test (Figure 3A). In the contextual and cued fear conditioning test, the freezing levels during the conditioning period ($P=0.4991$), context testing ($P=0.3353$), and the cued testing with altered context ($P=0.3285$) did not differ between the groups (Figure 3B).

Learning Test

In the working memory task of the 8-arm radial maze, sham-operated mice improved their performance over training, whereas BCAS mice did not and made significantly more errors than the sham-operated control ($P<0.0001$; 2-way repeated measures ANOVA; Figure 4A). The number of different arm choices in the first 8 entries is another measure of working memory performance. The number ranged from 5.3 for a chance performance to 8 for a perfect performance. However, sham-operated mice improved significantly more than BCAS mice with each consecutive training session ($P=0.0002$, 2-way repeated measures ANOVA; Figure 4B).

On the other hand, there were no significant differences between the groups in the reference memory task of the 8-arm radial maze ($F_{1,20}=2.878$, $P=0.1053$, 2-way repeated measures ANOVA; Figure 4C). After 8-arm radial maze test, the same animals were subjected to the open field test (Figure 4D through 4G). The activity level of BCAS mice was similar to the sham-operated mice (total distance; $F_{1,19}=0.050$,

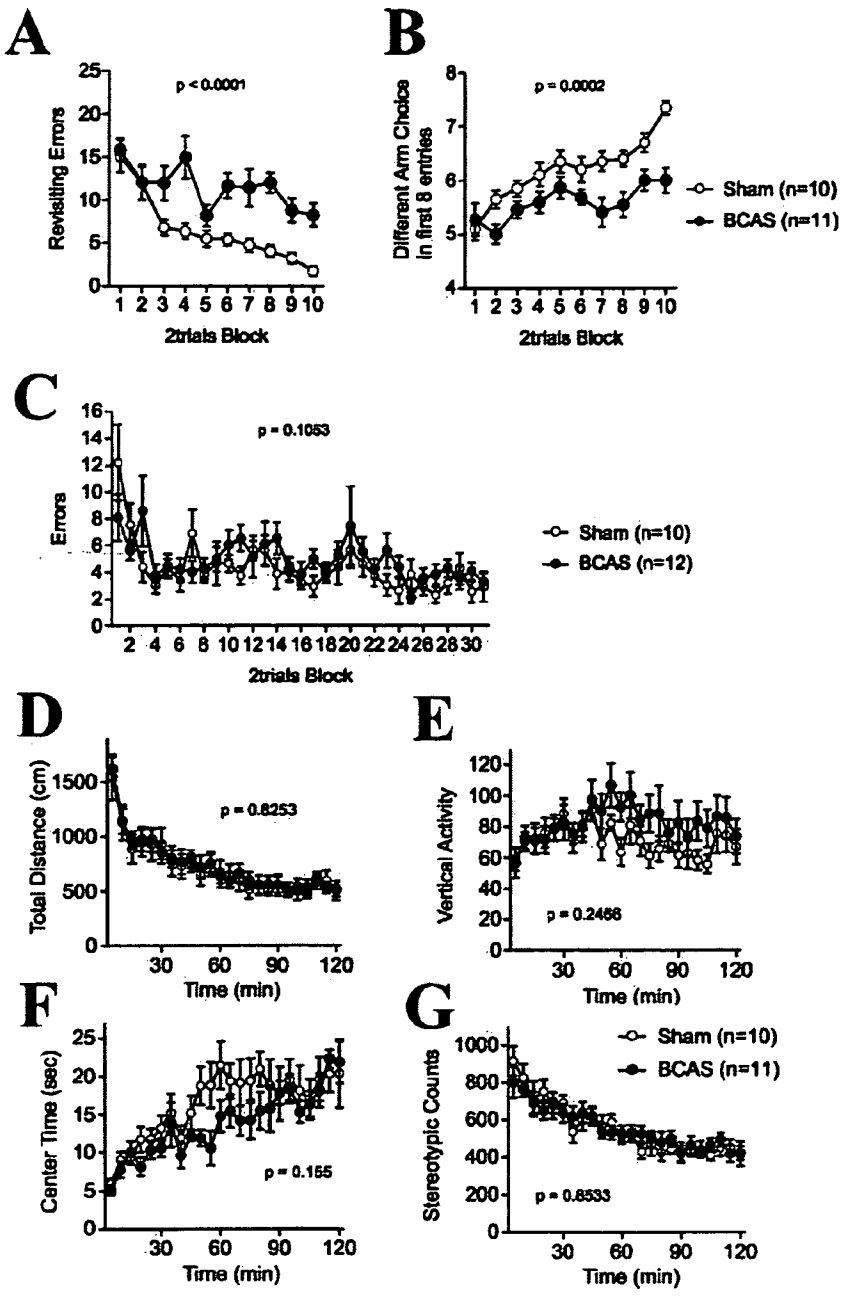

Figure 4. Working memory (A and B) and reference memory (C) of the control and BCAS mice in an 8-arm radial maze test. Data are given as means (±SEM) for revisiting errors (A), and different arm choices (B) in working memory task, and errors in reference memory task (C). BCAS mice showed a lesser number of different arm choices (group effect, $F_{1,19}=20.519$, $P=0.0002$; A), and more revisiting errors (group effect, $F_{1,19}=43.267$, $P<0.0001$; B) as compared with the control mice. There was no significant difference in the number of errors in reference memory task between the groups (group effect, $F_{1,20}=2.878$, $P=0.1053$; C). Locomotor activity of the control and BCAS mice in the open field test (D through G). No difference was observed for total distance (group effect, $F_{1,19}=0.050$, $P=0.8253$; D), vertical activity (group effect, $F_{1,19}=0.693$, $P=0.4155$; E), time spent in the center area (group effect, $F_{1,19}=2.194$, $P=0.155$; F), and the number of stereotypic counts (group effect, $F_{1,19}=0.002$, $P=0.9654$; G).

$P=0.8253$, 2-way repeated measures ANOVA). Thus, spatial reference memory required to correctly perform the reference memory task in the 8-arm radial maze does not appear to be affected in the BCAS mice.

Discussion

In the rat model of chronic cerebral hypoperfusion, although we did not find any changes in the hippocampus,[5] previous studies have reported hippocampal CA1 damages.[12,13] Hippocampal damages may cause impairment of both reference and working memory, and therefore make it difficult to determine whether the cognitive impairment was a consequence of WM lesions. Variability in hippocampal damage in the rat model may be caused by a relatively severe reduction of the CBF (30% to 50% of the preoperative values), in which low variability around the threshold may determine the occurrence of hippocampal changes.

In the current mouse model, if the degree of chronic cerebral hypoperfusion is appropriately controlled by changing the internal diameter of the microcoils, the decrease in CBF can be milder to selectively affect the cerebral WM. Using microcoils with a diameter of 0.16 mm, the CBF was decreased to 51.4±11.5% of the preoperative values with the resultant hippocampal CA1 damage.[11] However, using microcoils with a diameter of 0.18 mm or 0.20 mm, the CBF was decreased to 67.3±18.5% and 77.3±13.4%, respectively, and the histological damages including activation of microglia and astroglia were restricted to the WM.[11]

The BCAS mice showed no difference to the controls in the comprehensive behavioral tests, including a complete neurological screen, prepulse inhibition, hot plate, open field, light/dark transition, Porsolt forced swim and contextual and cued fear conditioning. Thus, this screen showed that these mice have no deficits in physical characteristics and sensory/motor functions. In addition, BCAS mice showed normal spatial reference memory in the 8-arm radial maze test. Spatial reference memory task was related to cognitive domains thought to rely on the integrity of the hippocampus, and therefore preserved reference memory is in agreement with lack of histological damage in the hippocampus. In contrast, working memory impairment may be attributable to either frontal WM lesions or hippocampal damages which are undetectable by the present methods. In previous studies, working memory deficits have been related either to the hippocampus or frontal-subcortical circuits in the rodent[14,19,20] and likely primates.[21,22] Therefore, the disruption of WM tracts especially within the prefrontal cortex may be another mechanism for age-related changes in working memory function.[23]

We successfully developed a mouse model of chronic cerebral hypoperfusion, which showed cognitive abnormalities with only a mild damage to the visual system. In the rat model, working memory and gait performances have been shown to be impaired.[12,13,24] However, the rat model exhibits severe degeneration and atrophy of the optic nerve.[5,14,25,26] The possibility cannot be ruled out that the visual system impairment may compromise the behavioral test, because visual cues contribute to discrimination even in the rodent.[27]

In this setting, the rat model is suitable for pharmacological evaluation because of prompt emergence of WM changes and easy applicability of stereotaxic surgery. In contrast, the mouse, which is readily amenable to gene knockout and manipulation and has advantages in cognitive evaluation, can be a model of subcortical vascular dementia suited for pathogenetic analysis and behavioral assessment.

Sources of Funding

This work was supported in part by a Grant-in-Aid for scientific research (C) (18590936) from the Japanese Ministry of Education, Culture, Sports, Science and Technology. This study is a part of joint research, which is focusing on the development of the basis of technology for establishing COE for nano-medicine, carried out through Kyoto City Collaboration of Regional Entities for Advancing Technology Excellence (CREATE) assigned by Japan Science and Technology Agency (JST).

Disclosures

None.

References

1. Roman GC, Erkinjuntti T, Wallin A, Pantoni L, Chui HC. Subcortical ischaemic vascular dementia. *Lancet Neurol.* 2002;1:426–436.
2. Fernando MS, Simpson JE, Matthews F, Brayne C, Lewis CE, Barber R, Kalaria RN, Forster G, Esteves F, Wharton SB, Shaw PJ, O'Brien JT, Ince PG; MRC Cognitive Function and Ageing Neuropathology Study Group. White matter lesions in an unselected cohort of the elderly: molecular pathology suggests origin from chronic hypoperfusion injury. *Stroke.* 2006;37: 1391–1398.
3. Kudo T, Tada K, Takeda M, Nishimura T. Learning impairment and microtubule-associated protein 2 decrease in gerbils under chronic cerebral hypoperfusion. *Stroke.* 1990;21:1205–1209.
4. Hattori H, Takeda M, Kudo T, Nishimura T, Hashimoto S. Cumulative white matter changes in the gerbil brain under chronic cerebral hypoperfusion. *Acta Neuropathol (Berl).* 1992;84:437–442.
5. Wakita H, Tomimoto H, Akiguchi I, Kimura J. Glial activation and white matter changes in the rat brain induced by chronic cerebral hypoperfusion: an immunohistochemical study. *Acta Neuropathol (Berl).* 1994;87:484–492.
6. Kurumatani T, Kudo T, Ikura Y, Takeda M. White matter changes in the gerbil brain under chronic cerebral hypoperfusion. *Stroke.* 1998;29: 1058–1062.
7. Tomimoto H, Ihara M, Wakita H, Ohtani R, Lin JX, Akiguchi I, Kinoshita M, Shibasaki H. Chronic cerebral hypoperfusion induces white matter lesions and loss of oligodendroglia with DNA fragmentation in the rat. *Acta Neuropathol (Berl).* 2003;106:527–534.
8. Lin J-Xi, Tomimoto H, Akiguchi I, Wakita H, Shibasaki H, Horie R. White matter lesions and alteration of vascular cell composition in the brain of spontaneously hypertensive rats. *Neuro Report.* 2001;12:1835–1839.
9. de Groot JC, de Leeuw FE, Oudkerk M, Hofman A, Jolles J, Breteler MMB. Cerebral white matter lesions and subjective cognitive dysfunction: The Rotterdam Scan Study. *Neurology.* 2001;56:1539–1545.
10. Tullberg M, Fletcher E, DeCarli C, Mungas D, Reed BR, Harvey DJ, Weiner MW, Chui HC, Jagust WJ. White matter lesions impair frontal lobe function regardless of their location. *Neurology.* 2004;63:246–253.
11. Shibata M, Ohtani R, Ihara M, Tomimoto H. White matter lesions and glial activation in a novel mouse model of chronic cerebral hypoperfusion. *Stroke.* 2004;35:2598–2603.
12. Ni JW, Matsumoto K, Li HB, Murakami Y, Watanabe H. Neuronal damage and decrease of central acetylcholine level following permanent occlusion of bilateral common carotid arteries in rat. *Brain Res.* 1995;673:290–296.
13. Tanaka K, Ogawa N, Asanuma M, Kondo Y, Nomura M. Relationship between cholinergic dysfunction and discrimination learning disabilities in Wistar rats following chronic cerebral hypoperfusion. *Brain Res.* 1996; 729:55–65.
14. Ohta H, Nishikawa H, Kimura H, Anayama H, Miyamoto M. Chronic cerebral hypoperfusion by permanent internal carotid ligation produces learning impairment without brain damage in rats. *Neuroscience.* 1997;79: 1039–1050.
15. Nakaji K, Ihara M, Takahashi C, Itohara S, Noda M, Takahashi R, Tomimoto H. MMP-2 play a critical role in the pathogenesis of white matter lesions after chronic cerebral hypoperfusion in rodents. *Stroke.* 2006;37:2816–2823.
16. Crawley JN. *What's Wrong With My Mouse? Behavioral Phenotyping of Transgenic and Knockout Mice.* New York, NY: Wiley-Liss; 2000.
17. Miyakawa T, Yamada M, Duttaroy A, Wess J. Hyperactivity and intact hippocampus-dependent learning in mice lacking the M1 muscarinic acetylcholine receptor. *J Neurosci.* 2001;21:5239–5250.
18. Miyakawa T, Leiter LM, Gerber DJ, Gainetdinov RR, Sotnikova TD, Zeng H, Caron MG, Tonegawa S. Conditional calcineurin knockout mice exhibit multiple abnormal behaviors related to schizophrenia. *Proc Natl Acad Sci U S A.* 2003;100:8987–8992.
19. Hiraga Y, Iwasaki T. Recent advances in studies of rat memory in the radial-arm maze. *Yakubutsu Seishin Kodo.* 1983;3:99–108.
20. Sarti C, Pantoni L, Bartolini L, Inzitari D. Cognitive impairment and chronic cerebral hypoperfusion: what can be learned from experimental models. *J Neurol Sci.* 2002; 203–204: 263–266.
21. Funahashi S, Bruce CJ, Goldman-Rakic PS. Mnemonic coding of visual space in the monkey's dorsolateral prefrontal cortex. *J Neurophysiol.* 1989;61:331–349.
22. Nordahl CW, Ranganath C, Yonelinas AP, Decarli C, Fletcher E, Jagust WJ. White matter changes compromise prefrontal cortex function in healthy elderly individuals. *J Cogn Neurosci.* 2006;18:418–429.
23. Burton EJ, Kenny RA, O'Brien J, Stephens S, Bradbury M, Rowan E, Kalaria R, Firbank M, Wesnes K, Ballard C. White matter hyperintensities are associated with impairment of memory, attention, and global cognitive performance in older stroke patients. *Stroke.* 2004;35:1270–1275.
24. Sarti C, Pantoni L, Bartolini L, Inzitari D. Persistent impairment of gait performances and working memory after bilateral common carotid artery occlusion in the adult Wistar rat. *Behav Brain Res.* 2002;136:13–20.
25. Takamatsu J, Hirano A, Levy D, Henkind P. Experimental bilateral carotid artery occlusion: a study of the optic nerve in the rat. *Neuropathol Appl Neurol.* 1984;10:423–428.
26. Davidson CM Pappas BA, Stevens WD, Fortin T, Bennett SAL. Chronic cerebral hypoperfusion: loss of pupillary reflex, visual impairment and retinal neurodegeneration. *Brain Res.* 2000;859:96–103.
27. Sutherland RJ, Hamilton DA. Rodent spatial navigation: at the crossroads of cognition and movement. *Neurosci Biobehav Rev.* 2004;28:687–697.

BRAIN RESEARCH 1135 (2007) 195–200

available at www.sciencedirect.com

ScienceDirect

www.elsevier.com/locate/brainres

BRAIN RESEARCH

Research Report

Expression of S100 protein and protective effect of arundic acid on the rat brain in chronic cerebral hypoperfusion

Ryo Ohtani, Hidekazu Tomimoto, Hideaki Wakita, Hiroshi Kitaguchi, Kayoko Nakaji, Ryosuke Takahashi*

Department of Neurology, Kyoto University Graduate School of Medicine, Shogoin, Sakyo-ku, Kyoto 606-8507, Japan

ARTICLE INFO

Article history:
Accepted 30 November 2006
Available online 8 January 2007

Keywords:
White matter
Chronic cerebral hypoperfusion
Apoptosis
Astroglia
S100 protein
Arundic acid

ABSTRACT

S100 protein is expressed primarily by astroglia in the brain, and accumulates in and around the ischemic lesions. Arundic acid, a novel astroglia-modulating agent, is neuroprotective in acute cerebral infarction, whereas the protective effects remain unknown during chronic cerebral hypoperfusion. Rats undergoing chronic cerebral hypoperfusion were subjected to a bilateral ligation of the common carotid arteries, and were allowed to survive for 3, 7 and 14 days. The animals received a daily intraperitoneal injection of 5.0, 10.0 or 20.0 mg/kg of arundic acid, or vehicle, for 14 days. Alternatively, other groups of rats received a delayed intraperitoneal injection of 20.0 mg/kg of arundic acid or vehicle, which started from 1, 3 or 7 days after ligation and continued to 14 days. The degree of white matter (WM) lesions and the numerical density of S100 protein-immunoreactive astroglia were estimated. In the WM of rats with vehicle injections, the number of S100 protein-immunoreactive astroglia increased significantly after chronic cerebral hypoperfusion as compared to the sham-operation. A dosage of 10.0 and 20.0 mg/kg of arundic acid suppressed the numerical increase in S100 protein-immunoreactive astroglia and the WM lesions. These pathological changes were suppressed with delayed treatment up to 7 days in terms of astroglial activation, and up to 3 days in terms of the WM lesions. The protective effects of arundic acid against WM lesions were demonstrated in a dose-dependent manner, and even after postischemic treatments. These results suggest the potential usefulness of arundic acid in the treatment of cerebrovascular WM lesions.

1. Introduction

Ischemic white matter (WM) lesions are frequently observed in human cerebrovascular diseases (CVD), and are believed to be responsible for cognitive impairments in the elderly. It is believed that the occlusion of the small vessels results in lacunar cerebral infarction, and non-occlusive arteriopathy causes chronic cerebral hypoperfusion and WM lesions (Pantoni and Garcia, 1997). Indeed, WM lesions can be induced by a ligation of the bilateral common carotid arteries (CCAs) in rats, which leads to a 50–70% decrease in normal cerebral blood flow (CBF) over an extended period of time (Tsuchiya

* *Corresponding author.* Fax: +81 75 751 3766.
E-mail address: tomimoto@kuhp.kyoto-u.ac.jp (H. Tomimoto).

Abbreviations: WM, white matter; CVD, cerebrovascular disease; CCAs, common carotid arteries; CBF, cerebral blood flow; iNOS, inducible nitric oxide synthase; PBS, phosphate-buffered saline; KB, Klüver–Barrera; BBB, blood–brain barrier; TNFα, tumor necrosis factor alpha; COX2, cyclooxygenase 2

0006-8993/$ – see front matter © 2006 Elsevier B.V. All rights reserved.
doi:10.1016/j.brainres.2006.11.084

et al., 1992; Wakita et al., 1994). The myelins become rarefied with a proliferation of the astroglia and an activation of microglia, plus oligodendroglial cell death with DNA fragmentation in the WM (Tomimoto et al., 2003).

S100 is a 20-kDa Ca-binding protein composed of α and β subunits, and is primarily expressed by astroglia in the brain. This protein may play a dual role in the regulation of cell function, being beneficial to cells at low doses but detrimental at high doses (Hu et al., 1996). In human CVD, a significant correlation has been reported between the plasma concentration of S100 protein and the volume of the cerebral infarct (Aurell et al., 1991). Although low concentrations of S100 protein protect cultured neurons from glutamate-induced excitotoxic damage, a high concentration of this protein upregulates the expression of inducible nitric oxide synthase (iNOS) in cultured astroglia with the subsequent production of NO and death of astroglia and neurons (Hu et al., 1996, 1997; Murphy, 2000).

Indeed, arundic acid, an agent that inhibits the astrocytic synthesis of S100 (Asano et al., 2005), has been shown to be neuroprotective in a rat model of acute cerebral infarction (Tateishi et al., 2002). Arundic acid may interfere with the intricate pathways of astrocytic activation upstream to the mRNA expression of various proteins, and is considered to be a modulator of the gene expression and functions of astroglia (Asano et al., 2005; Shinagawa et al., 1999).

In the present study, we examined the protective effects of arundic acid on WM lesions during chronic cerebral hypoperfusion, and also investigated its therapeutic window for delayed treatment. Our results support the potential use of arundic acid as a therapeutic intervention in human cerebrovascular WM lesions with cognitive impairment.

2. Results

2.1. *Mortality rates and laboratory data*

In the first series of experiments, 1 out of 7 arundic acid-treated rats died at a dosage of 5.0 mg/kg (14.3%), and none died at dosages of 10.0 and 20.0 mg/kg (0.0%). The laboratory data (erythrocyte count, leukocyte count, GOT, GPT, BUN and creatinine levels) and rectal temperature were not significantly different between the vehicle-treated and arundic acid-treated rats (Table 1).

2.2. *Dose-dependent effect of arundic acid on S100 protein expression*

In the WM of the sham-operated animals, only a few astroglia showed positive immunostaining for the S100 protein. From 3 to 14 days after the operation, the brains of the vehicle-treated animals showed a numerical increase in astroglia, which were immunoreactive for S100 protein in various WM regions such as the optic nerve, optic tract, corpus callosum, and internal capsule (Figs. 1A–D). These S100 protein-immunoreactive astroglia increased in number after BCAO as compared to the sham-operated control group in these WM regions (Fig. 1E, Table 2).

In the 10.0 and 20.0 mg/kg arundic acid-treated rats, S100 protein-immunoreactive astroglia appeared to be less numerous in the WM regions as compared to the vehicle-treated animals for 14 days. In the semi-quantitative analysis, the number of S100 protein-immunoreactive astroglia was reduced in both 10.0 and 20.0 mg/kg arundic acid-treated groups as compared to the vehicle-treated group ($p<0.001$; Figs. 2A–D). The number of astroglia decreased in the 5.0, 10.0 and 20.0 mg/kg arundic acid-treated groups compared to the vehicle-treated group. The number was also reduced in the 20.0 mg/kg arundic acid-treated animals as compared to the 10.0 mg/kg arundic acid-treated animals ($p<0.05$), indicating a dose-dependent effect for arundic acid (Fig. 2E, Table 2).

2.3. *Dose-dependent effect of arundic acid on WM lesions*

This dose-related protective effect was similarly observed with respect to the WM lesions. In the 10.0 and 20.0 mg/kg arundic acid-treated groups, the scores were lower as compared to the vehicle-treated group (two-factor factorial ANOVA; $p<0.001$). There were no significant differences in grading scores between the 5.0 mg/kg arundic acid-treated group and vehicle-treated group. However, the 20.0 mg/kg arundic acid-treated animals showed a significant reduction ($p<0.05$) as compared to the 10.0 mg/kg arundic acid-treated animals (Fig. 2F, Table 2).

2.4. *Effects of delayed treatment*

In the delayed-treatment group, which started from 1, 3, or 7 days after the operation, the number of S100 protein-immunoreactive astroglia showed a significant decrease in the WM regions as compared to the vehicle-treated animals

Table 1 – Summary of the laboratory data in rats receiving vehicle or arundic acid

	Erythrocyte ($\times 10^4$/mm^3) (n=6)	Leukocyte ($\times 10^2$/mm^3) (n=6)	Thrombocyte ($\times 10^3$/mm^3) (n=6)	GOT (IU/l) (n=5)	GPT (IU/l) (n=6)	BUN (mg/dl) (n=5)	Creatinine (mg/dl) (n=6)	Rectal temperature (°C) (n=6)
Vehicle	753.0±42.8	48.4±8.6	88.6±9.6	156.8±18.8	53.6±6.6	20.4±2.8	0.48±0.08	36.5±0.5
Arundic acid (5.0 mg/kg)	790.0±36.8	52.5±22.8	90.4±10.8	178.6±20.4	49.6±8.8	21.8±2.2	0.54±0.12	36.6±1.0
Arundic acid (10.0 mg/kg)	778.0±20.4	50.8±16.8	92.4±9.6	148.8±22.4	45.2±6.8	18.6±1.9	0.46±0.09	36.5±1.0
Arundic acid (20.0 mg/kg)	774.4±31.8	54.8±18.6	91.4±14.4	166.6±38.4	51.2±9.2	19.8±2.4	0.52±0.14	36.6±0.5

Values represent means±SD. n, number of animals. No significant differences were detected in the laboratory data between the arundic acid-treated group and the vehicle-treated group.

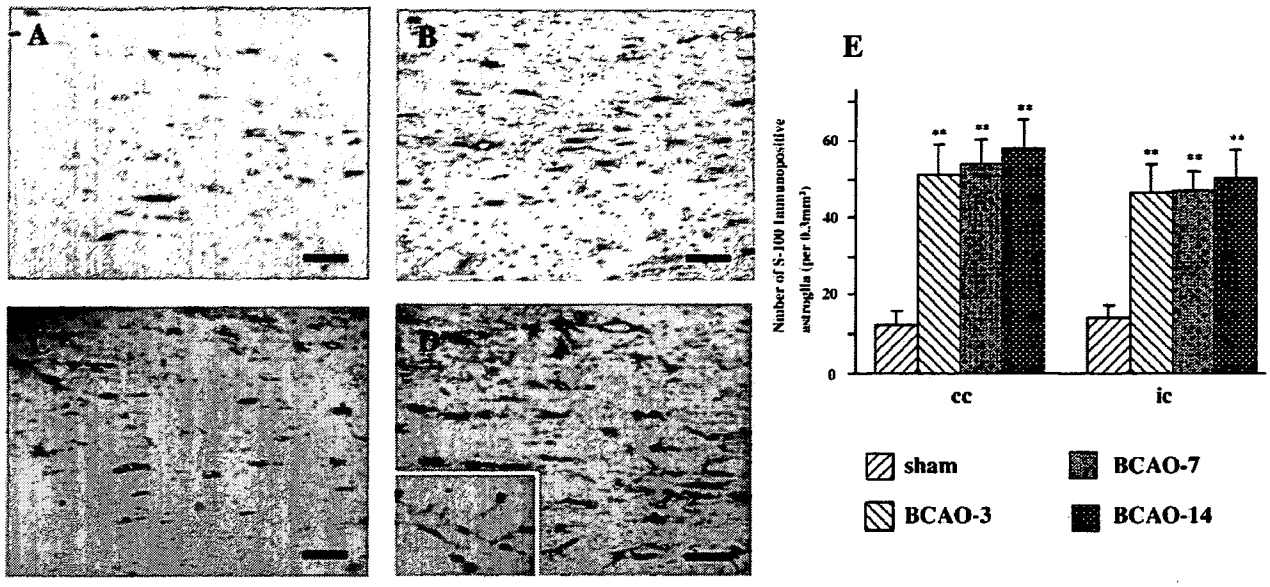

Fig. 1 – Photomicrographs of the immunohistochemical staining for S100 protein in the corpus callosum. The rats were subjected to a sham operation (A), or bilateral ligation of the carotid arteries for 3 days (B), 7 days (C) or 14 days (D). An inset in (D) indicates that S100 protein is intensely expressed in astroglial foot processes around the blood vessel. Bars indicate 100 μm. E: Histograms of the numerical densities of S100 protein-immunoreactive astroglia in the WM of the rats after a bilateral common carotid artery occlusion. Six animals were used in each group. The asterisks indicate statistical significance at $p<0.01$ by Mann–Whitney *U* test when compared with the sham-operated controls. cc, corpus callosum; ic, internal capsule.

for 14 days (Figs. 3A–E, Table 2). The WM lesions were less severe (two-factor factorial ANOVA; $p<0.001$) as compared to the vehicle-treated group in the groups starting at 1 day and 3 days after the operation (Fig. 3F, Table 2), but there were no significant changes in the group starting at 7 days.

3. Discussion

In the present study, we demonstrated a protective effect for arundic acid against astroglial activation and WM lesions during chronic cerebral hypoperfusion. Arundic acid suppressed both the activation of the astroglia and the WM lesions in a dose-dependent manner. Both the astroglial activation and WM lesions were suppressed at dosages over 10 mg/kg, whereas the dosage of 5.0 mg/kg suppressed the astroglial activation exclusively. Therefore, it is unlikely that the activation of the astroglia was secondary to the WM damage, but rather seems to be related to the causative mechanism.

Microglia and astroglia are activated in the WM aberrantly after chronic cerebral hypoperfusion (Wakita et al., 1994). This activation occurs in a manner that predicts the extent and severity of the subsequent WM damage, suggesting an important role of glial activation in the pathogenesis of WM lesions. In the susceptible WM, apoptosis of the oligodendroglia is induced with an upregulation of inflammatory cytokines including tumor necrosis factor alpha (TNFα), and free radicals released from activated microglia and astroglia (Tomimoto et al., 2003). In addition, the compromised BBB (Ueno et al., 2002) may allow the entry of macromolecules and other blood constituents such as proteases, immunoglobulins, complements, and cytokines into the perivascular WM tissues.

In studies using a neuronal and astroglia co-culture system, a high concentration of S100 protein upregulated NO release from the astroglia, which was shown to be neurotoxic

Table 2 – The number of S100 protein-immunoreactive astroglia in the white matter

	Corpus callosum				Internal capsule			
I. Temporal profile after BCAO	Sham	3 days	7 days	14 days	Sham	3 days	7 days	14 days
	12.3±3.5	51.3±7.8**	53.8±6.9**	58.1±7.3**	14.0±3.6	46.5±7.7**	47.0±5.2**	50.5±7.1**
II. Dose-dependent effect	Vehicle	5 mg/kg	10 mg/kg	20 mg/kg	Vehicle	5 mg/kg	10 mg/kg	20 mg/kg
	63.5±8.3	53.1±6.3**	35.3±6.2**	10.9±6.0**	54.9±8.4	33.0±7.1**	26.1±5**	21.9±5.7**
III. Effects of delayed treatment	Vehicle	Day 1	Day 3	Day 7	Vehicle	Day 1	Day 3	Day 7
	62.0±6.6	13.2±3.8**	18.2±5.1**	48.9±6.6**	54.5±7.1	21.9±3.1**	23.7±5.0**	42.2±6.3**

Values represent the number of S100 protein-immunoreactive astroglia in 0.3 mm^2 (means±SD).
** $p<0.01$ compared to the sham-operated (I) and the vehicle-treated (II and III) animals.

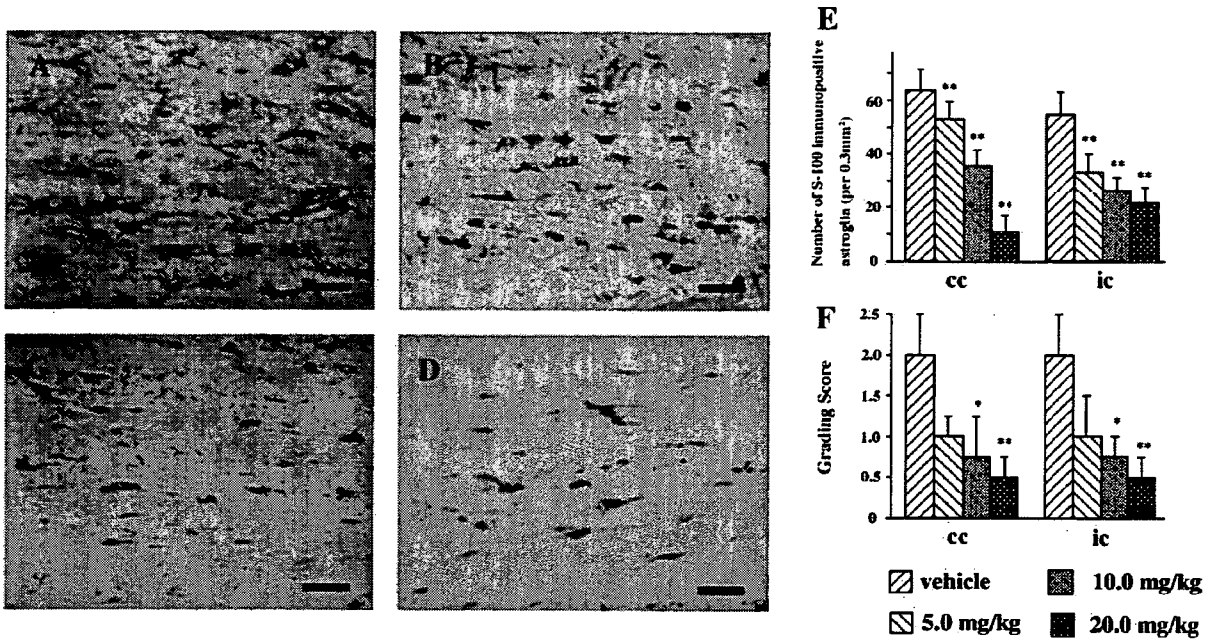

Fig. 2 – Photomicrographs of the immunohistochemical staining for S100 protein in the corpus callosum. The animals received an intraperitoneal injection of vehicle (A) or 5.0 mg/kg (B), 10.0 mg/kg (C) and 20.0 mg/kg (D) of arundic acid for 14 days. In the arundic acid-treated animals, astroglia immunoreactive for S100 protein were less numerous as compared with the vehicle-treated animals. Bars indicate 100 μm. The histograms show the numerical densities of S100 protein-immunoreactive astroglia (E), and the grading scores for the WM lesions (F) in rats receiving either vehicle or arundic acid for 14 days. *$p<0.05$; **$p<0.01$ by Fisher's protected least significant difference procedure, as compared to the vehicle-treated animals.

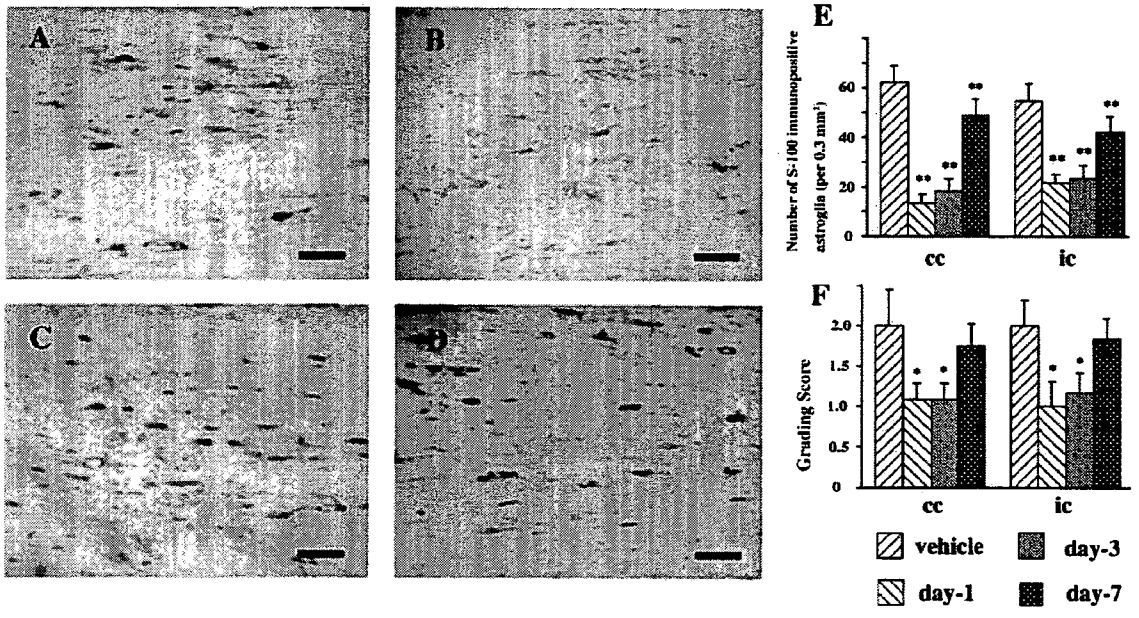

Fig. 3 – Photomicrographs of the immunohistochemical staining for S100 protein in the corpus callosum. The animals received an intraperitoneal injection of 20.0 mg/kg of arundic acid from 1 day (B), 3 days (C) or 7 days (D) after the operation, until 14 days. The control animals (A) received a daily injection of vehicle 1 day before the operation until 14 days. In the delayed treatment with arundic acid, the number of S100 protein-immunoreactive astroglia was significantly reduced as compared with the control animals. Bars indicate 100 μm. The histograms show the numerical density of S100 protein-immunoreactive astroglia (E) and the grading scores for the WM lesions (F) in rats receiving either vehicle or arundic acid from 1 day, 3 days or 7 days after the operation until 14 days. *$p<0.05$; **$p<0.01$ by Fisher's protected least significant difference procedure, as compared to the vehicle-treated animals.

(Hu et al., 1997; Nawashiro et al., 2000). Although the mechanism of responsible for this astroglial activation by a low concentration of S100 protein remains unclear, this protein is believed to be further activated by a positive feedback loop (Guo et al., 2001; Murphy, 2000). It is postulated that these excessively activated astroglia may cause secondary tissue damage by the production of cytotoxic cytokines such as TNFα, and cyclooxygenase 2 (COX2) and iNOS (Lam et al., 2001; Sharp et al., 2000). Indeed, the delayed expansion of the cerebral infarction was accompanied by astroglial activation as well as by an increased tissue level of S100 protein in the peri-infarct area. Thus, the astroglial overexpression of S100 protein is considered to play a pivotal role in infarct expansion by causing alterations in the activities of multiple intracellular signaling pathways and the expression of various downstream proteins (Asano et al., 2005; Matsui et al., 2002).

Several *in vitro* and *in vivo* studies have determined the pharmacological actions of arundic acid on astroglia. Arundic acid acts selectively on astroglia and modulates their activation, or prevents excessive activation that may be harmful to neighboring neurons. It does not act on neuronal cultures directly, but suppresses the changes induced in the co-cultured astroglia, such as an increase in S100β content, the secretion of nerve growth factor, a reduction in glutamate transporter (GLT-1 and GLAST) expression and the disappearance of GABAA receptors, in a dose-dependent manner, without affecting GFAP expression (Asano et al., 2005; Himeda et al., 2006; Katsumata et al., 1999; Matsui et al., 2002). In addition, arundic acid inhibits the expression of cyclooxygenase-2 or inducible nitric oxide synthase mRNA induced by lipopolysaccharide in cultured astroglia (Shimoda et al., 1998).

The dosage ranging from 5 to 20 mg/kg in the present study was comparable to that used in clinical application (8 mg/kg/h in acute stroke patients) (Pettigrew et al., in press). Furthermore, arundic acid was effective in delayed treatment starting from 7 days in terms of astroglial activation, and 3 days in terms of the WM lesions. This broad therapeutic time window is of clinical relevance, because the patients with subcortical vascular dementia, a form of vascular dementia characterized by diffuse WM lesions, frequently undergo a latent deterioration and hospitalization delay (Roman, 2005).

4. Experimental procedures

4.1. *Animals*

Chronic cerebral hypoperfusion was induced in male Wistar rats (150 to 200 g; Shimizu Laboratory Supplies Co. Ltd., Kyoto, Japan) as previously described (Wakita et al., 1994). The animals were anesthetized with sodium pentobarbital (25 mg/kg, i. p.) and were allowed spontaneous respiration throughout the surgical procedure. Through a midline cervical incision, both CCAs were exposed and double-ligated with silk sutures. Their rectal temperature was monitored and maintained between 36.0 and 37.0 °C during the surgical procedure, and the rats were kept in animal quarters with standard rodent chow and tap water *ad libitum* after the operation.

4.2. *Treatment with arundic acid*

The rats with vehicle (saline) treatment were sacrificed at 3, 7 and 14 days (body weight, 300 g; $n=6$, for each group) to study the temporal profile of the S100 protein-immunoractive astroglia and the WM lesions. In the first series of experiments with arundic acid, the animals received a daily intraperitoneal injection of 5.0, 10.0 or 20.0 mg/kg of arundic acid, or vehicle, from 1 day before the operation to 14 days afterwards ($n=6$ for each group). At 14 days after ligation, the animals were sacrificed and subjected to the experiments detailed below. The sham-operated animals were treated similarly to the operated ones, except the CCAs were not occluded. In the second series with a delayed-treatment, the animals received a daily intraperitoneal injection of 20.0 mg/kg of arundic acid or vehicle from 1 day, 3 days or 7 days after the operation until 14 days ($n=6$ for each group). At 14 days after ligation, the animals were sacrificed and subjected to the experiments detailed below. The control animals received a daily injection of vehicle 1 day after the operation until 14 days.

4.3. *Standard histological and immunohistochemical study*

After the operation, the animals were deeply anesthetized with sodium pentobarbital and were perfused transcardially with 0.01 mol/L phosphate-buffered saline (PBS), and then with a fixative containing 4% paraformaldehyde and 0.2% picric acid in 0.1 mol/L PB (pH 7.4). The brains were then stored in 20% sucrose in 0.1 mol/L PBS (pH 7.4). These specimens were embedded in paraffin and sliced into 2 μm-thick coronal sections. Klüver–Barrera (KB) staining was used to observe any histological changes. The severity of the WM lesions was graded as normal (grade 0), disarrangement of the nerve fibers (grade 1), formation of vacuoles (grade 2) and loss of myelinated fibers (grade 3) by two independent investigators blinded to the type of treatment, as described elsewhere (Wakita et al., 1994). For the immunohistochemistry, polyclonal antibodies directed against the S100 protein (diluted 1:1000; Dakopatts, 4.5 mg/L) were used in the present study. After incubation with the primary antibodies, the sections were treated with a biotinylated anti-rabbit antibody (IgG) (diluted 1:200; Vector Laboratories), and an avidin biotin complex (diluted 1:200; Vector Laboratories) in 20 mmol/L PBS containing 0.3% Triton-X. The sections were finally incubated in 0.01% diaminobenzidine tetrahydrochloride and 0.005% H_2O_2 in 50 mmol/L Tris HCl (pH 7.6). To test the specificity of the immunohistochemical reaction, coronal sections were treated with normal mouse IgG instead of the primary antibodies. The number of nuclei with S100 protein-immunoreactive cytoplasm was counted against a square test grid in 20 representative fields (per 0.3 mm^2) of the corpus callosum and internal capsule ($n=6$) by two independent investigators blinded to the type of treatments as described previously (Tomimoto et al., 1996).

4.4. *Statistical analysis*

The data were expressed as means±SD. Differences in rectal temperature between the groups were determined by a

repeated-measure ANOVA. Differences in terms of laboratory blood data were determined by a one-factor ANOVA between each group. Differences in the grading scores were determined by a two-factor factorial ANOVA followed by Fischer's protected least significant difference procedure between each group. The Kruskal–Wallis test followed by post-hoc test was used to compare the ischemic group with the sham-operated control group in the semiquantification for S100 protein-immunoreactive astroglia. A p value of <0.05 was considered to be statistically significant.

Acknowledgments

We appreciatively acknowledge Ono Pharmaceutical Co. Ltd., Osaka, Japan, for providing arundic acid (ONO-2506), and for helpful advice. This study was supported by a grant-in-aid for scientific research (C) (18590936) from the Japanese Ministry of Education, Culture, Sports, Science and Technology to H. T. and Dr. H. Saiki (Kitano Hospital, Osaka, Japan).

REFERENCES

Asano, T., Mori, T., Shimoda, T., Shinagawa, R., Satoh, S., Yada, N., Katsumata, S., Matsuda, S., Kagamiishi, Y., Tateishi, N., 2005. Arundic acid (ONO-2506) ameliorates delayed ischemic brain damage by preventing astrocytic overproduction of S100B. Curr. Drug Targets, CNS Neurol. Disord. 4, 127–142.

Aurell, A., Rosengren, E.L., Larlsson, B., Olsson, E.J., Zbornikova, V., Haglid, G.K., 1991. Determination of S-100 and glial fibrillary acidic protein concentrations in cerebrospinal fluid after brain infarction. Stroke 22, 1254–1258.

Guo, L., Sawkar, A., Zasadzki, M., Watterson, M.D., 2001. Similar activation of glial cultures from different rat brain regions by neuroinflammatory stimuli and downregulation of the activation by a new class of small molecule ligands. Neurobiol. Aging 22, 975–981.

Himeda, T., Kadoguchi, N., Kamiyama, Y., Kato, H., Maegawa, H., Araki, T., 2006. Neuroprotective effect of arundic acid, an astrocyte-modulating agent, in mouse brain against MPTP (1-methyl-4-phenyl-1,2,3,6-tetrahydropyridine) neurotoxicity. Neuropharmacology 50, 329–344.

Hu, J., Castets, F., Guevana, L.J., 1996. S100β stimulates inducible nitric oxide synthase activity and mRNA levels in rat cortical astrocytes. J. Biol. Chem. 271, 2543–2547.

Hu, J., Ferreia, A., 1997. S100β induces neuronal cell death through nitric oxide release from astrocytes. J. Neurochem. 69, 2294–2301.

Katsumata, S., Tateishi, N., Kagamiishi, Y., Shintaku, K., Hayakawa, T., Shimoda, T., Shinagawa, R., Akiyama, T., Katsube, N., 1999. Inhibitory effect of ONO-2506 on GABAA receptor disappearance in cultures astrocytes and ischemic brain. Abstr.-Soc. Neurosci. 25, 2108.

Lam, G.A., Koppal, T., Akama, T.K., Guo, L., Craft, M.J., Samy, B., Schavocky, P.J., Watterson, M.D., 2001. Mechanism of glial activation by S100B: involvement of the transcription factor NF κB. Neurobiol. Aging 22, 765–772.

Matsui, T., Mori, T., Tateishi, N., Kagamiishi, Y., Satoh, S., Katsube, N., Morizawa, E., Morimoto, T., Ikuda, F., Asano, T., 2002. Astrocytic activation and delayed infarct expansion after permanent focal ischemia in rats. Part 1: enhanced astrocytic synthesis of S100β in the periinfarct area precedes delayed infarct expansion. J. Cereb. Blood Flow Metab. 22, 711–722.

Murphy, S., 2000. Production of nitric oxide by glial cells: regulation and potential roles in the CNS. Glia 29, 1–13.

Nawashiro, H., Brenner, M., Fukui, S., Shima, K., Hallenbeck, M.J., 2000. High susceptibility to cerebral ischemia in GFAP-null mice. J. Cereb. Blood Flow Metab. 20, 1040–1044.

Pantoni, H.J., Garcia, H.J., 1997. Pathogenesis of leukoaraiosis: a review. Stroke 28, 652–659.

Pettigrew, C.L., Kasner, E.S., Albers, W.G., Gorman, M., Grotta, C.J., Sherman, G.D., Funakoshi, Y., Ishibashi, H., for the arundic acid (ONO-2506) stroke study group, 2006. Safety and tolerability of arundic acid in acute ischemic stroke. J. Neurol. Sci. 251, 50–56.

Roman, C.G., 2005. Vascular dementia prevention: a risk factor analysis. Cerebrovasc. Dis. 20, 91–100.

Sharp, R.F., Lu, A., Tang, Y., Millhorn, E.D., 2000. Multiple molecular penumbras after focal cerebral ischemia. J. Cereb. Blood Flow Metab. 20, 1011–1032.

Shimoda, T., Tateishi, K., Shintaku, K., Yada, N., Katagi, J., Akiyama, T., Maekawa, H., Shinagawa, R., Kondo, K., 1998. ONO-2506, a novel astrocyte modulating agent, suppresses of COX-2 and iNOS mRNA expression in cultured astrocytes and ischemic brain. Abstr.-Soc. Neurosci. 24, 384.

Shinagawa, R., Tateishi, N., Shimoda, T., Maekawa, H., Yada, N., Akiyama, T., Matsuda, S., Katsube, N., 1999. Modulating effects of ONO-2506 on astrocytic activation in cultured astrocytes from rat cerebrum. Abstr.-Soc. Neurosci. 25, 843.

Tateishi, N., Mori, T., Kagamiishi, Y., Satoh, S., Katsube, N., Morizawa, E., Morimoto, T., Matsui, T., Asano, T., 2002. Astrocytic activation and delayed infarct expansion after permanent focal ischemia in rats. part 2: suppression of astrocytic activation by a novel agent (R)-(–)-2-propyloctanoic acid (ONO-2506) leads to mitigation of delayed infarct expansion and early improvement of neurologic deficits. J. Cereb. Blood Flow Metab. 22, 723–734.

Tomimoto, H., Akiguchi, I., Suenaga, T., Nishimura, M., Wakita, H., Nakamura, S., Kimura, J., 1996. Alterations of the blood-brain barrier and glial cells in white matter lesions in cerebrovascular and Alzheimer's disease patients. Stroke 27, 2069–2074.

Tomimoto, H., Ihara, M., Wakita, H., Ohtani, R., Lin, X.J., Akiguchi, I., Kinoshita, M., Shibasaki, H., 2003. Chronic cerebral hypoperfusion induces white matter lesions and loss of oligodendroglia with DNA fragmentation in the rat. Acta Neuropathol. (Berl.) 106, 527–534.

Tsuchiya, M., Sako, K., Yura, S., Yonemasu, Y., 1992. Cerebral blood flow and histopathological changes following permanent bilateral carotid artery ligation in Wistar rats. Exp. Brain Res. 89, 87–92.

Ueno, M., Tomimoto, H., Akiguchi, I., Wakita, H., Sakamoto, H., 2002. Blood-brain barrier is disrupted in the white matter lesions in a rat model of chronic cerebral hypoperfusion. J. Cereb. Blood Flow Metab. 22, 97–104.

Wakita, H., Tomimoto, H., Akiguchi, I., Kimura, J., 1994. Glial activation and white matter changes in the rat brain induced by chronic cerebral hypoperfusion: an immunohistochemical study. Acta Neuropathol. (Berl.) 87, 484–492.